


## Temporally precise control of single-neuron spiking by juxtacellular nanostimulation

 Maik C. Stüttgen,<sup>1,2,3\*</sup> Lourens J. P. Nonkes,<sup>1\*</sup> H. Rüdiger A. P. Geis,<sup>1,4</sup> Paul H. Tiesinga,<sup>5</sup> and Arthur R. Houweling<sup>1</sup>

<sup>1</sup>Department of Neuroscience, Erasmus University Medical Center, Rotterdam, The Netherlands; <sup>2</sup>Institute of Pathophysiology, University Medical Center of the Johannes Gutenberg University, Mainz, Germany; <sup>3</sup>Focus Program Translational Neuroscience, Johannes Gutenberg University, Mainz, Germany; <sup>4</sup>Neuronal Networks Group, German Center for Neurodegenerative Diseases, Bonn, Germany; and <sup>5</sup>Department of Neuroinformatics, Donders Centre for Neuroscience, Radboud University Nijmegen, Nijmegen, The Netherlands

Submitted 13 June 2016; accepted in final form 9 January 2017

**Stüttgen MC, Nonkes LJ, Geis HR, Tiesinga PH, Houweling AR.** Temporally precise control of single-neuron spiking by juxtacellular nanostimulation. *J Neurophysiol* 117: 1363–1378, 2017. First published January 11, 2017; doi:10.1152/jn.00479.2016.—Temporal patterns of action potentials influence a variety of activity-dependent intra- and intercellular processes and play an important role in theories of neural coding. Elucidating the mechanisms underlying these phenomena requires imposing spike trains with precisely defined patterns, but this has been challenging due to the limitations of existing stimulation techniques. Here we present a new nanostimulation method providing control over the action potential output of individual cortical neurons. Spikes are elicited through the juxtacellular application of short-duration fluctuating currents (“kurzpulses”), allowing for the sub-millisecond precise and reproducible induction of arbitrary patterns of action potentials at all physiologically relevant firing frequencies (<120 Hz), including minute-long spike trains recorded in freely moving animals. We systematically compared our method to whole cell current injection, as well as optogenetic stimulation, and show that nanostimulation performance compares favorably with these techniques. This new nanostimulation approach is easily applied, can be readily performed in awake behaving animals, and thus promises to be a powerful tool for systematic investigations into the temporal elements of neural codes, as well as the mechanisms underlying a wide variety of activity-dependent cellular processes.

**NEW & NOTEWORTHY** Assessing the impact of temporal features of neuronal spike trains requires imposing arbitrary patterns of spiking on individual neurons during behavior, but this has been difficult to achieve due to limitations of existing stimulation methods. We present a technique that overcomes these limitations by using carefully designed short-duration fluctuating juxtacellular current injections, which allow for the precise and reliable evocation of arbitrary patterns of neuronal spikes in single neurons *in vivo*.

juxtacellular stimulation; whole cell; optogenetics, cortex

THE SPIKE TRAINS OF CORTICAL neurons are highly irregular (Softky and Koch 1993). It is well established that the temporal

patterns of neuronal spike trains convey information about the dynamics of sensory stimuli, in both peripheral and subcortical structures (Chagas et al. 2013; Johnson 1980; Reinagel and Reid 2000), as well as in cortical areas (Arabzadeh et al. 2006; Bair and Koch 1996; Kayser et al. 2010). The question of whether and how the brain extracts the temporal information contained in spike trains is an unresolved and highly debated issue that lies at the heart of our understanding of neural codes (Shadlen and Newsome 1998). Beyond the question of neural coding, it has become clear that the timing of neuronal spikes affects a variety of activity-dependent processes within cells, including intracellular signaling (Svoboda and Yasuda 2006), gene expression (Fields et al. 2005), homeostatic plasticity (Goold and Nicoll 2010), structural plasticity (Wyatt et al., 2012), and dendritic development (McAllister 2000), as well as processes that affect postsynaptic cells, including synaptic transmission (Tsodyks and Markram 1997), spike timing-dependent plasticity (Bi and Poo 1998; Froemke et al. 2006), and development of synaptic connectivity (Stellwagen and Shatz 2002).

A crucial step toward clarifying the role of temporal patterns requires imposing arbitrary spike trains on neurons in anesthetized and awake animals. It has been difficult to make this important first step, due to limitations in the ability to manipulate neural activity using existing techniques. Current mass stimulation approaches, such as microstimulation and photostimulation, induce an unknown number of spikes in an unknown number of neurons, both directly and indirectly through synaptic interactions, because these approaches lack a read-out mechanism. Thus, to precisely characterize the effects of temporal spike patterns, techniques are required that combine stimulation and recording with single-cell and single-spike resolution. In its most rudimentary form, such a technique would involve the stimulation of single neurons. Despite the elementary scale of perturbation, single-cell stimulation exerts a measurable influence on spike generation in neighboring neurons (Kwan and Dan 2012; London et al. 2010; Rickgauer et al. 2014), movement (Brecht et al. 2004), global brain state (Li et al. 2009), and even sensation (Houweling and Brecht 2008). Moreover, the recent finding that single-cell stimulation in sensory cortex

\* M. C. Stüttgen and L. J. P. Nonkes contributed equally to this work.

Address for reprint requests and other correspondence: M. C. Stüttgen, Institute of Pathophysiology, University Medical Center Mainz, Hanns-Dieter-Hüsch-Weg 19, 55128 Mainz, Germany (e-mail: maik.stuetzgen@uni-mainz.de).

elicits behavioral responses that vary with spike train irregularity (Doron et al. 2014), as well as the ability of single-cell stimulation to elucidate phenomena such as hippocampal place field formation (Bittner et al. 2015; Diamantaki et al. 2016; Lee et al. 2012), demonstrate the power of the single-cell stimulation approach for addressing fundamental questions on the neural code.

Whole cell recording, in principle, provides a method to precisely drive neuronal spikes through injection of brief current steps (Brecht et al. 2004) or fluctuating currents constructed from filtered white noise (Mainen and Sejnowski 1995). However, whole cell recording has a few methodological drawbacks that limit its applicability *in vivo*. Recent advances in *in vivo* whole cell recording techniques notwithstanding, recordings are limited to only few sessions per animal (Domnisoru et al. 2013; Haider et al. 2013). In addition, intracellular substances are washed out of the cell during standard whole cell recording, complicating studies of intracellular signaling mechanisms. Moreover, despite recent progress, it is still technically challenging to obtain stable whole cell recordings in awake behaving animals (Epszstein et al. 2011; Sachidhanandam et al. 2013).

To address some of these issues, our laboratory recently reestablished the juxtacellular nanostimulation technique (Houweling et al. 2010). Nanostimulation is technically less challenging than whole cell stimulation because the juxtacellular recording configuration does not require breaking into the cell, and pipettes can be used repeatedly to target individual neurons. Also, the dura can be left in place, which is essential for chronic preparations. Most importantly, the technique is readily applicable to trained, awake behaving animals: each animal can be used multiple times over many weeks to collect recordings from neurons (Doron et al. 2014; Houweling and Brecht 2008). However, up to now, the technique did not provide precise control over the number and timing of spikes elicited in single neurons recorded *in vivo*.

Here we describe a single-cell nanostimulation approach for imposing arbitrary spike trains on neurons using short-duration fluctuating juxtacellular current injections. To illustrate the technological advance, we present several demonstrations. First, we show that single action potentials can be reliably evoked (>95% success rate) with high precision (~0.5 ms spike time jitter) in cortical neurons *in vivo*. Second, we demonstrate that trains of spikes can be faithfully induced at all physiologically relevant firing frequencies (up to 120 Hz). Third, we show that the technique can be used to impose an arbitrary pattern of action potentials, using minute-long segments of spikes recorded in freely moving animals. Finally, we assess the reliability and precision of *in vivo* whole cell stimulation and optogenetic stimulation and show that nanostimulation compares favorably with these techniques.

## METHODS

**Ethical approval.** All experiments were approved by the Dutch animal experiment ethical committee and in accordance with the Institutional Animal Care and Use Committee guidelines.

**Subjects and surgery.** Twenty-five C57BL/6J mice of both sexes (15 females, 10 males) aged from 68 to 205 days (mean 149) served as subjects. A subset of experiments was performed in transgenic Arc::dVenus mice backcrossed more than 10 generations into C57BL/6J (Eguchi and Yamaguchi 2009). These mice expressed a

destabilized fluorescent protein (dVenus) under the control of a bacterial artificial chromosome transgenic *Arc* promoter, leaving the endogenous *Arc* genes unmodified. These mice function as a fluorescence-based reporter of endogenous *Arc* transcription without interfering with the function of *Arc* itself. Fluorescence was not quantified in the present study. No differences were found between males and females, or wild-type and transgenic mice, and all data were therefore collapsed. Mice were kept on a 12:12-h light-dark cycle with food and water available *ad libitum*. Experiments were conducted during the light phase.

At the onset of experiments, animals were anesthetized by intraperitoneal injection of 20% urethane dissolved in saline (1 ml/100 g body wt). The head was fixed using a custom-built head-plate attached to the skull with dental acrylic. A rectangular craniotomy was performed above S1 cortex (0–2 mm posterior, 2–4 mm lateral from bregma), and the brain surface was covered by Ringer solution containing the following (in mM): 135 NaCl, 5.4 KCl, 1.0 MgCl<sub>2</sub>, 1.8 CaCl<sub>2</sub>, 5.0 HEPES (pH 7.2).

**Juxtacellular recordings.** Glass pipettes (outer diameter 1.5 mm; Hilgenberg) were pulled on a horizontal micropipette puller (P-97, Sutter Instrument) to a tip opening of 1–2 μm and a resistance of 4–7 MΩ. Pipettes were filled with intracellular solution containing the following (in mM): 126 potassium-gluconate, 10 HEPES (pH 7.2), 10 Na<sub>2</sub>-phosphocreatine, 20 KCl, 4 Mg-ATP, 0.3 Na<sub>2</sub>-GTP, and EGTA 0.5. In pilot experiments, we used Ringer solution containing the following (in mM): 135 NaCl, 5.4 KCl, 5 HEPES, 1.8 CaCl<sub>2</sub>, and 1 MgCl<sub>2</sub> (pH 7.2). We did not observe any obvious differences between recording sessions using either pipette solution. Voltage signals were amplified and low-pass filtered at 3 kHz with a patch-clamp amplifier (BVC-700A), and sampled at 20 kHz by a Power 1401 data acquisition interface (Cambridge Electronic Design) controlled via Spike2 software. Nanostimulation current injections were delivered at a 10-kHz sampling rate.

**Current pulse waveform identification.** Previous nanostimulation experiments have exclusively used rectangular current pulses for spike induction. These pulses produce substantial artifacts during pulse onset and offset, precluding reliable, automated spike detection for ~2 ms at the beginning and end of current injections (Houweling et al. 2010). When using current pulses on the order of hundreds of milliseconds, this procedure yields negligible false negative (miss) rates. However, when aiming for temporally precise induction of single spikes, one requires high current amplitudes during a short time window of only a few milliseconds, rendering rectangular pulses unsuitable. Figure 1A shows both raw and band-pass filtered voltage traces recorded from a neuron during a 2-ms and 10-ms rectangular nanostimulation pulse. Spontaneous spikes unrelated to current pulses were of high amplitude for this neuron (>5 mV in the unfiltered trace) and clearly visible in both unfiltered and filtered recordings (Fig. 1, B and C). Notably, the rectangular nanostimulation pulse had a small amplitude (1 nA), which is insufficient to drive spiking in nearly all cells from which we have recorded (even if maintained for 200 ms), but nevertheless the resulting artifact was large enough to occlude spikes from the recorded neuron. Moreover, the magnitude of the artifact scaled with current pulse amplitude. Thus, to evoke single action potentials at high temporal precision (<1-ms spike time jitter), we needed to design a current pulse waveform that is both short and whose frequency spectrum does not overlap with that of neuronal spikes.

In a series of pilot experiments, we tested a range of pulse waveforms, including Gaussians and cosines of varying duration. We found that a 500-Hz cosine wave (on the interval  $[-\pi, \pi]$ , i.e., 2-ms duration), low-pass filtered at 150 Hz (finite impulse response filter implemented in Spike2, function ArrFilt with 511 coefficients (FIRQuick), transition gap 0.1, 80-dB attenuation in stop band), provided excellent stimulation capabilities while inducing negligible artifacts (maximum observed artifact size was ~0.2 mV). Resulting waveforms (“kurzpulses”; Fig. 1B) were trimodal with two small

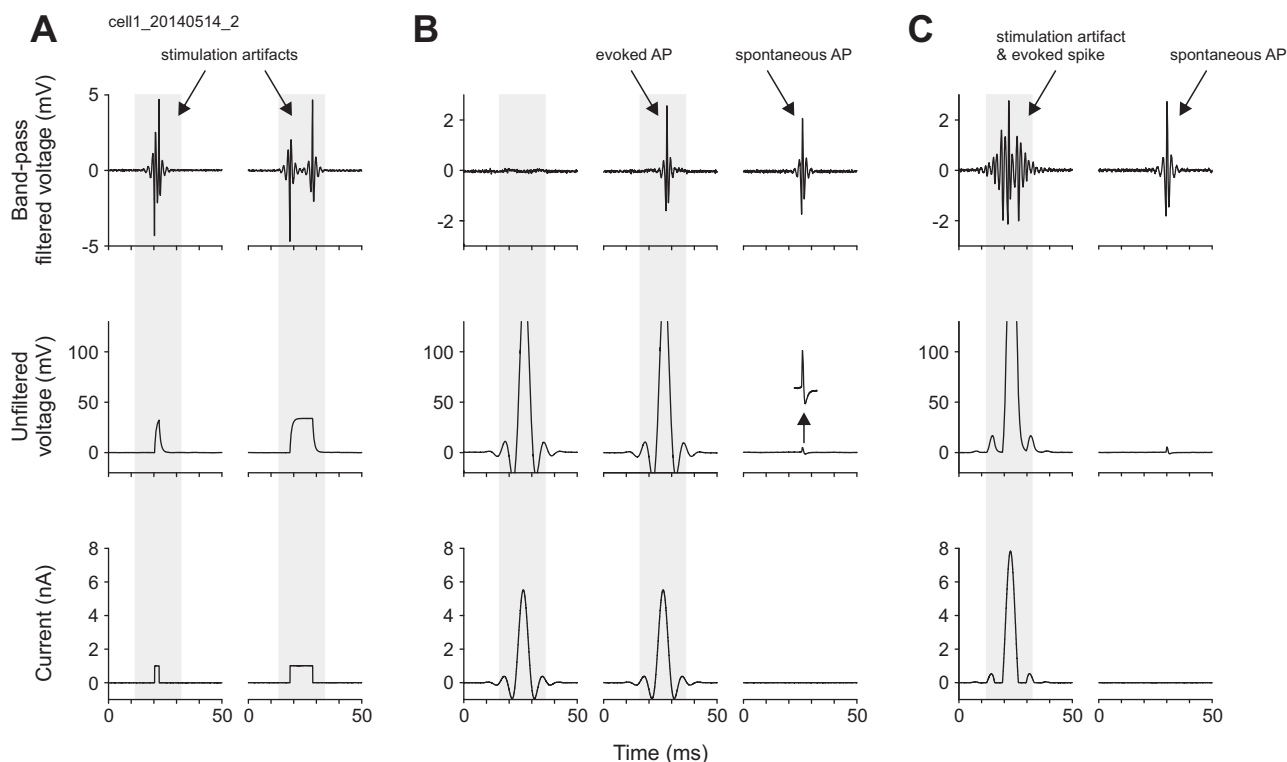


Fig. 1. Kurzpuls nanostimulation enables artifact-free single action potential (AP) induction. *A*: standard rectangular current pulses evoke recording artifacts large enough to mask simultaneously occurring spikes. *Bottom*: two example rectangular current pulses (*left*: 2-ms duration, *right*: 10-ms duration). *Middle*: raw voltage signal recorded simultaneously from the same electrode. *Top*: band-pass filtered voltage signal (500–5,000 Hz) used for AP extraction. Artifacts at stimulus onset and offset prevent spike identification. In this and the following panels, the shaded area serves to indicate stimulus occurrence. *B*: juxtacellular kurzpuls current injections are capable of eliciting APs while inducing negligible stimulation artifacts. *Bottom*: two example kurzpuls with current amplitudes close to threshold ( $I = 6$  nA). *Left*: kurzpuls with current peak of 5.5 nA that failed to evoke an AP, illustrating the absence of a stimulation artifact (*top*); *middle*, kurzpuls with the same amplitude that triggered an AP. *Right*: spontaneous AP to demonstrate the close similarity of evoked and spontaneous spike waveforms (*top*). *Inset* is shown at the same time scale but with 8-fold magnified y-axis. *C*: negative deflections flanking kurzpuls are not necessary to elicit spiking, but their exclusion yields stimulation artifacts. *Bottom*: rectified kurzpuls with negative current values clipped to 0 (delivered at 8 nA). Data in *A–C* are from the same neuron. Data in *B* were obtained during threshold determination for this unit.

humps flanking a third, much larger bell-shaped pulse that was  $\sim 7$  ms wide [note that the cosine function is not crucial, low-pass filtering a 2-ms direct current (DC) pulse will yield a very similar waveform]. For the neuron shown in Fig. 1, the amplitude of the kurzpuls needed to evoke single action potentials was severalfold higher than that of the rectangular pulse shown in Fig. 1*A* (5.5 nA vs. 1 nA), yet the evoked spike waveform is virtually identical to that of spontaneous spikes (Fig. 1*B*, *top*), implying a lack of artifacts.

For the generation of pulse sequences, cosine pulses were placed at the desired temporal positions and all together low-pass filtered as described above. Because our low-pass filter is linear, this procedure is equivalent to summing individual kurzpuls traces placed at the desired temporal positions. When generating Poisson sequences (see Fig. 4), we implemented a minimum time interval of 7 ms between subsequent cosine pulses before low-pass filtering, as summation of near-instantaneous kurzpuls leads to high current levels that might damage neurons.

**Kurzpuls nanostimulation.** After penetrating the dura, the pipette was left in place for approximately 5 min to allow for tissue relaxation. The pipette was subsequently advanced in steps of  $2 \mu\text{m}$  using a micromanipulator (Luigs and Neumann, Ratingen, Germany), while monitoring a current injection search pulse (1 nA, 200 ms on/off) until a rapid increase in resistance indicated the presence of a nearby cell. The pipette was slowly advanced until the DC resistance exceeded  $15\text{--}20 \text{ M}\Omega$  (Houweling et al. 2010). At that time, we first assessed the spontaneous firing rate for a few minutes and then continued to determine the minimum current necessary to reliably drive single spikes. Kurzpuls were delivered at 0.4 Hz, starting with a current

amplitude of 1 nA, which was increased by 0.5 nA after two consecutive failures to induce spiking. Threshold current ( $T$ ) was defined as the lowest current amplitude for which four spikes were evoked during four consecutive kurzpuls. Following  $T$  determination, one of several stimulation protocols (see RESULTS) commenced. Occasionally, individual neurons were confronted with another protocol; in these cases, the  $T$  was redetermined between protocols, and kurzpuls amplitude was adjusted accordingly.

As shown in earlier DC nanostimulation experiments (Houweling et al. 2010),  $T$  current amplitude was affected by the quality of the cell-pipette contact, as indicated by a negative relationship between  $T$  and total electrical impedance (total resistance  $R_T$  equals the ratio of the voltage deflection  $\Delta V$  over injected current amplitude  $\Delta I$ ,  $R_T = \Delta V/\Delta I$ , measured from trough-to-peak during kurzpuls current injections;  $r = -0.54$ ,  $P = 0.0085$ ; based on  $n = 23$  kurzpuls experiments shown in Fig. 3).  $R_T$  was on average  $23.6 \text{ M}\Omega$  (median  $20.4 \text{ M}\Omega$ , range  $15.5\text{--}42 \text{ M}\Omega$ ; based on  $n = 23$  kurzpuls experiments shown in Fig. 3) and varied little during experiments, as indicated by its coefficient of variation (CV) (mean 0.036; range: 0.0091–0.079). Occasionally, we observed sudden shifts in the recorded potential, increased firing rates, and increased responsiveness to electrical stimulation while running the stimulation protocol, probably due to membrane rupture leading to a quasi-intracellular recording configuration. In such cases, neurons usually died within several seconds; in other instances, neurons would recover after interruption of the stimulation protocol and could be driven to fire again. Data from such sessions was not included.

**Whole cell recordings.** Superficial layer 2 somatosensory cortex neurons were patched under two-photon guidance (custom setup with Mai Tai laser at 800 nm; Spectra-Physics) with glass pipettes (1–2  $\mu\text{m}$  tip; Hilgenberg) containing the following (in mM): potassium-glucuronate 138, KCl 8,  $\text{Na}_2$ -phosphocreatine 10, Mg-ATP 4,  $\text{Na}_2$ -GTP 0.3, EGTA 0.5, HEPES 10 (pH 7.2). Alexa Fluor 594 (40  $\mu\text{M}$ ; Invitrogen) and biocytin (0.5%; Sigma-Aldrich) were added to the internal solution for visualization of the pipette and histological recovery of the recorded neurons, respectively. The brain surface was stabilized with agar (2% in Ringer; Sigma-Aldrich) before the pipette was advanced into the brain. Pressure was reduced from 30 to 3 kPa while approaching layer 2. Whole cell current clamp recordings were amplified with a MultiClamp 700A (10-kHz low-pass Bessel filter), digitized at 25 kHz with a Digidata 1440A, and acquired with Clampex 10.2 (all Molecular Devices). Resting membrane potential was not corrected for junction potential and ranged from  $-64$  to  $-74$  mV with an average of  $-68$  mV. Measurements were done with an average access resistance of 38 M $\Omega$  (ranging from 27 to 59 M $\Omega$ ). Membrane resistance was on average 71 M $\Omega$  and ranged from 50 to 93 M $\Omega$ . Pipette capacitance neutralization and bridge balance were adjusted, and the spike T was determined as for juxtacellular recordings. Current intensity was increased by 50 pA until the neuron fired consistently in response to each of four consecutive 5-ms square pulse current injections presented at 0.4 Hz. The resulting T value was used in subsequent current amplitude and pulse train experiments.

**Optogenetic stimulation.** Mice were anesthetized using isoflurane (5% induction, 2–3% maintenance), and placed in a stereotaxic frame. A custom-built head-plate was attached to the skull using light-curable dental adhesive (OptiBond FL, Kerr), and a craniotomy was made over S1 cortex (center: 1.5 mm posterior, 3 mm lateral to bregma). Adeno-associated virus expressing channelrhodopsin-2 under the humanized synapsin promoter [AAV2/2-hSyn-ChR2(H134R)-EYFP; 250–500 nl;  $10^{13}$  copies/ml; UNC Vector Core] was pressure-injected in the center of the craniotomy at a depth of 200–500  $\mu\text{m}$ . Initial attempts with ChETA channelrhodopsin, which is characterized by very fast channel kinetics (Lin 2011), failed to yield robust cellular responses in our hands, even at maximum light intensity. The craniotomy was sealed using kwik-cast sealant (WPI) and dental acrylic. Rimadyl (Carprofen, 5 mg/kg) was administered subcutaneously as a postoperative analgesic.

After at least 4 wk postsurgery (range 4–13 wk), mice were anesthetized using 20% urethane. An optical fiber was positioned directly above the exposed cortical surface at a 45° angle, allowing a glass pipette to enter the brain for simultaneous juxtacellular recordings. The optical fiber was attached to a high-power 470-nm LED (M470F1, Thorlabs; 10.1 mW delivered through a 400- $\mu\text{m}$  diameter core, i.e., 80.4 mW/mm<sup>2</sup> near the brain surface). The LED driver (LEDD1B, Thorlabs) was controlled via a Power 1401 and Spike2 software (10-kHz sampling rate). Once juxtacellular recordings were established (as described above), the minimum light intensity to reliably drive single spikes was determined. To this aim, 7-ms light pulses were delivered at 0.4 Hz, starting with 5% of maximum light intensity. Intensity was thereafter increased in steps of 5% after every two consecutive failures to induce spiking. Threshold (T) was defined as the lowest light intensity at which four spikes were evoked during four consecutive light pulses. All subsequent photostimulation experiments were performed at 100% light intensity (maximum output power of the LED).

In a subset of experiments, *N*-methyl-D-aspartate receptor antagonist amino-5-phosphonopentanoate (APV, 1.6 mM) and  $\alpha$ -amino-3-hydroxy-5-methyl-4-isoxazolepropionic acid receptor antagonist 6-cyano-7-nitroquinoxaline-2,3-dione (CNQX, 0.8 mM) were applied onto the cortical surface to minimize indirect activation of the recorded neurons. In a previous study, these dosages completely suppressed light-evoked postsynaptic responses in mice expressing channelrhodopsin-2 (ChR2) (Mateo et al. 2011). Application of APV and

CNQX was also highly effective in our experiments, as it almost completely abolished spontaneous firing in recorded neurons.

**Analysis and statistics.** Juxtacellular recordings were filtered using a digital finite impulse response filter, with a passband of 500–5,000 Hz and a 200-Hz transition gap to stopbands (>60 dB attenuation). Spikes were extracted from the filtered voltage signal by detecting peaks whose amplitude exceeded a threshold. Reported spike times refer to the peak times of the filtered spike waveforms. Correct spike extraction was visually confirmed for all nanostimulation experiments, whole cell recordings, and photostimulation experiments.

Analysis windows for computing success rate, doublet rate, spike onset latency, and spike time jitter were of 7-ms duration and centered on the kurzpuls peak, thus capturing the central positive phase and ignoring the low-amplitude flanks. Longer analysis windows (10 or 14 ms) had negligible effects on the results. For the whole cell and optogenetics data, we extended the duration of the analysis window to 10 ms (whole cell) and 14 ms (optogenetics) to capture the occasional spikes induced immediately after stimulation offset. All statistical analyses (*t*-test, analysis of variance, Pearson correlation; significance threshold set to 0.05) were conducted in Matlab (The MathWorks).

## RESULTS

A glass pipette was advanced through the intact dura of urethane-anesthetized mice until a neuron was encountered in S1 cortex. We sought to construct current waveforms that would allow reliable and temporally precise (<1 ms spike time jitter) induction of individual action potentials in the juxtacellular recording configuration. Previous studies mostly used 200-ms rectangular depolarizing current pulses to evoke action potentials (“DC nanostimulation”; Houweling et al. 2010). However, application of rectangular pulses induces two large, steep voltage jumps in the recording (Fig. 1A), which preclude reliable spike detection during onset and offset for a total period of 2–4 ms per pulse, even after band-pass filtering (see artifacts in *top* panel). Moreover, these pulse waveforms offer only limited control over the number and firing frequency of evoked spikes (Houweling et al. 2010). We found that a low-pass filtered (<150 Hz) cosine current pulse with a full width at half maximum of 3–4 ms (Fig. 1B, *bottom*) induces negligible artifacts in the frequency band of neuronal spikes and is capable of inducing action potentials that are indistinguishable from spontaneously occurring spikes (Fig. 1B, *top*). The resultant current waveform (henceforth referred to as “kurzpuls,” which is German for “short pulse”) resembles a Mexican hat function. The main positive peak is flanked by short segments of negative current waves: these segments are not necessary to evoke temporally precise neuronal spikes, but their omission results in the reappearance of stimulation artifacts (Fig. 1C; data not shown).

In a series of experiments, we assessed the reliability of the stimulation method and its ability to evoke spikes with high temporal precision. In all experiments, we first gradually increased the amplitude of kurzpulses in steps of 0.5 nA until four neuronal spikes were evoked by four consecutive stimuli delivered at 0.4 Hz (we refer to this current intensity as threshold T). Following T determination (median 6.5 nA, range 2.5–17 nA), neurons were confronted with one or more of several stimulation protocols. We targeted neurons across all cortical layers (depth meter range 152–1,210  $\mu\text{m}$ , mean 787  $\mu\text{m}$ , SD 285  $\mu\text{m}$ ). None of our neurons featured narrow-width action potential waveforms (Houweling and Brecht 2008) characteristic of parvalbumin-expressing fast-spiking interneurons,

suggesting that the vast majority of our cells were of the excitatory type.

**Current amplitude dependence.** To assess the reliability and temporal precision of kurzpuls nanostimulation, as well as their dependence on current amplitude, we tested 12 cortical cells with different current intensities, expressed as a fraction of  $T$  ( $0.8 \leq T \leq 1.6$ ). Figure 2A shows a spike raster for an example neuron recorded at a depth of  $526 \mu\text{m}$  below the cortical surface. Three observations can be made. First, success rate (defined as the fraction of trials in which at least one spike was evoked) is high throughout with the exception of the below-threshold current intensity of  $0.8 T$ . Second, the latency of the evoked spike (relative to the kurzpuls peak) progressively shortens as current increases. Third, spike time jitter (defined as the standard deviation of first-

spike latencies) decreases with increasing current, in line with results from in vitro whole cell recordings employing fluctuating current injections (Mainen and Sejnowski 1995). Similar observations were made for all 12 cells in our data set. On average, success rate increased with current intensity and remained larger than 0.95 at values of  $T > 1.1$  ( $F_{6,66} = 9.5$ ,  $P < 10^{-6}$ ; Fig. 2B). Occasionally, single kurzpuls evoked two spikes; however, the average rate of evoked spike doublets was consistently  $<0.05$  for all tested current intensities (Fig. 2C). Spikes were evoked with high temporal precision, with the average spike onset latency (time of evoked spike relative to pulse maximum) increasing from roughly  $-0.5$  ms for high- to  $+0.5$  ms for low-current values ( $F_{6,66} = 10.2$ ,  $P < 10^{-9}$ ; Fig. 2D), and spike time jitter was consistently below 1 ms (Fig. 2E). Although spike

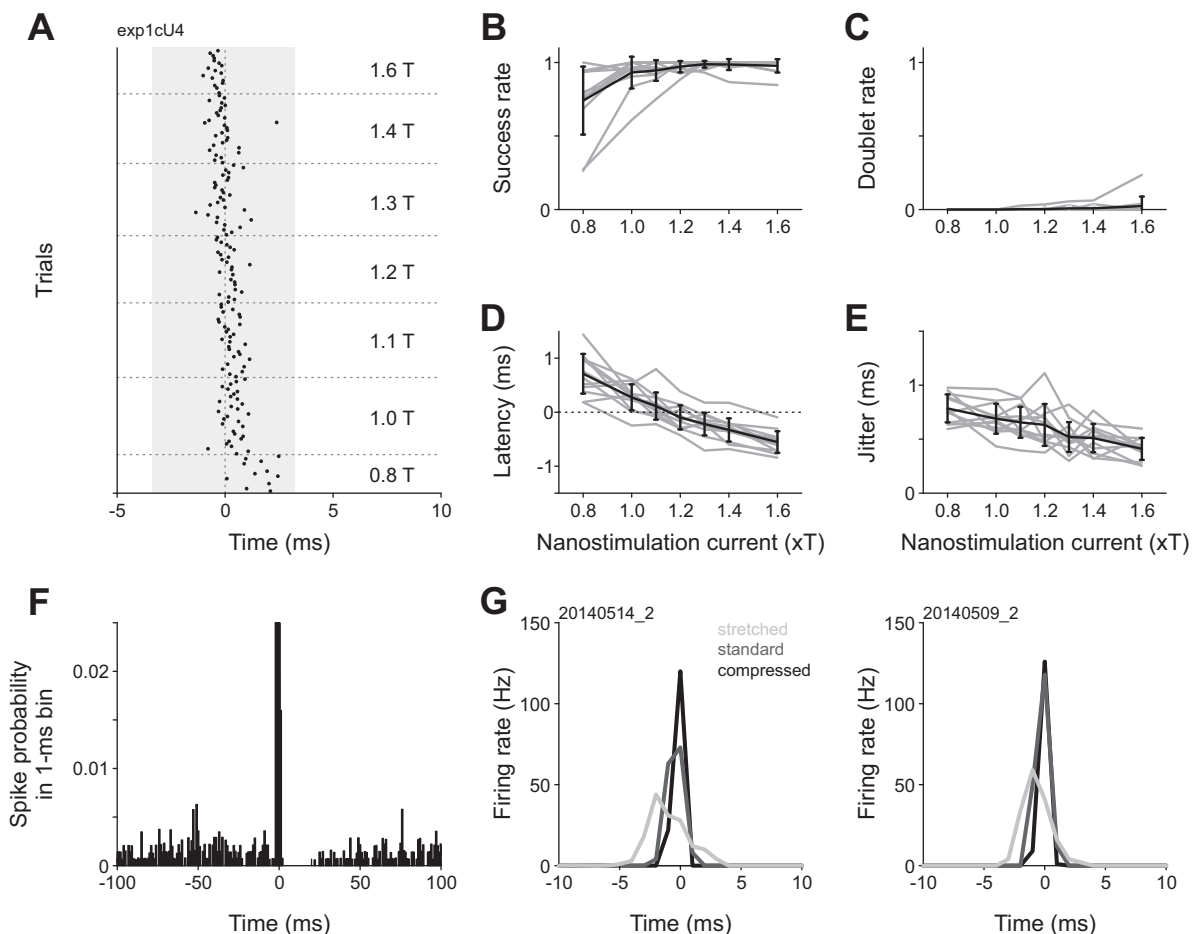


Fig. 2. Current amplitude dependence of spike induction by kurzpuls nanostimulation. **A**: spike raster for an example neuron stimulated with kurzpuls of different amplitudes. Stimuli were presented in pseudorandom sequence (repetition rate 0.4 Hz), but are sorted for display purposes. Current amplitudes are expressed as a factor of threshold current  $T$  (8.5 nA for this neuron). Shading indicates the extent of the central positive peak of the kurzpuls (duration 7.0 ms, see Fig. 1B). **B**: fraction of trials in which kurzpuls nanostimulation evoked one or more spikes inside a 7-ms analysis window centered on the kurzpuls peak (“success rate”) as a function of nanostimulation current. Shaded lines: individual neurons, solid line: success rate averaged over  $n = 12$  cells. Error bars denote standard deviation. **C**: fraction of trials in which kurzpuls nanostimulation evoked two or more spikes (“doublet rate”). Conventions in **C–E** are the same as in **B**. **D**: spike onset latency (relative to kurzpuls peak); positive values indicate that spikes lagged the pulse peak. **E**: spike time jitter, computed as the standard deviation of first spikes evoked by the kurzpuls. **F**: average PSTH of 10 neurons centered on kurzpuls peaks (1.3 T, repetition rate 0.4 Hz). Bin size, 1 ms. Ordinate was truncated (PSTH extends up to a probability of  $\sim 0.7$ ). **G**: PSTHs from two cells exposed to modified kurzpuls of different widths. Kurzpuls waveforms were modified by changing the output sampling rate (standard 10 kHz), resulting in either compressed (20 kHz) or stretched (5 kHz) waveforms. Single pulses were delivered at 1.3 T with a repetition rate of 0.4 Hz. Thresholds were determined separately for each waveform ( $T$  values, cell 1: 5.5, 7.0, 9.5 nA; cell 2: 5.0, 5.0, 9.5 nA for stretched, standard, and compressed kurzpuls, respectively). Analysis windows extended from  $-3.5$  to  $+3.5$  ms relative to the kurzpuls peaks. Success rates were equally high for all waveforms ( $>0.97$ ), whereas doublet rates were 0 except for the stretched kurzpuls presented to cell 1 (0.13). Spike time jitter was 1.2 (1.0), 0.6 (0.5), and 0.2 (0.3) ms for stretched, standard, and compressed kurzpuls for the cell on the left and right, respectively. Data on the left are from the neuron depicted in Fig. 1.

time jitter decreased up to current intensities of 1.6 T ( $F_{6,66} = 14.4$ ,  $P < 10^{-9}$ ), we decided to perform subsequent experiments at 1.3 T because we observed that high current intensities increased the risk of cell damage (as indicated by a sudden increase in responsivity to stimulation current, a decrease in electrical resistance, and an increase of spike amplitude).

In two other cells, we assessed how reliability and temporal precision depend on temporal aspects of the kurzpuls. In these experiments, we presented both standard and modified kurzpuls waveforms that were either compressed (with half the standard width) or stretched in time (with double the standard width). Success rates were equally high for all waveforms ( $>0.97$ ), while spike time jitter increased proportionally to kurzpuls width (Fig. 2G). Although compressed kurzpulses resulted in lower spike time jitter, we decided to perform subsequent experiments with regular kurzpulses because compression reintroduced stimulation artifacts in the recordings and required larger T currents.

**Spontaneous neural firing.** Ideally, a single-spike induction technique should not alter spontaneous firing after spike induction. Previously, we observed that DC nanostimulation occasionally increased firing for a brief period directly following stimulation (Houweling et al. 2010). The reason for this is unknown, but one possibility is that the membrane depolarization induced by juxtacellular current injections outlasts the stimulation pulse. To investigate whether kurzpuls nanostimulation affects spontaneous firing, we recorded the activity of 10 cells during a stimulus sequence consisting of single suprathreshold (1.3 T) kurzpulses delivered at 0.4 Hz. Figure 2F shows an average peristimulus time histogram (PSTH) of spiking activity centered on kurzpuls peaks. Surprisingly, we found that the firing rate following kurzpulses is reduced rather than elevated for a period of  $\sim 20$ –50 ms ( $t_0 = 3.8$ ,  $P = 0.004$ ,

paired *t*-test), as can also be observed following sensory stimulation eliciting single spikes (DeWeese et al. 2003; Stüttgen and Schwarz 2008). This reduced firing could be the result of several nonexclusive mechanisms: first, inactivation of sodium channels underlying action potential generation; second, activation of voltage-gated and/or calcium-dependent potassium currents; third, inhibitory synaptic “feedback” inputs from interneurons recruited by the stimulated cell (Kwan and Dan 2012); and fourth, negative current injection as part of the kurzpuls (directly following the central positive peak). The latter is highly unlikely because we did not observe reduced firing during the negative current injection directly preceding the central kurzpuls peak (Fig. 2F). Importantly, the brief paucity does not indicate absolute refractoriness; below, we will show that kurzpuls nanostimulation is capable of inducing additional action potentials for interpulse intervals  $< 10$  ms.

**Induction of regular spike trains.** The above experiments set the ground for more systematic investigations of spike patterns imposed through kurzpuls nanostimulation. As a next step, we stimulated 23 neurons with sequences of 10 kurzpulses delivered at 5, 10, 20, 40, 80, and 120 Hz (6 of these neurons were tested only with frequencies 5–40 Hz). In particular, we were interested to see whether spikes could be driven reliably under these conditions with respect to success rate and spike time jitter, and whether these parameters differed across stimulation frequencies. Figure 3A shows a spike raster for an example cell; Fig. 3, B–D shows average results. Generally speaking, success rate was very high for all 10 pulses at all frequencies, with a slight reduction at very high stimulation frequencies (80 and 120 Hz). The reduced success rates at 80- and 120-Hz stimulation frequencies might be due to superposition of neighboring kurzpuls waveforms, which was not compensated for. Due to this superposition of positive and negative portions of

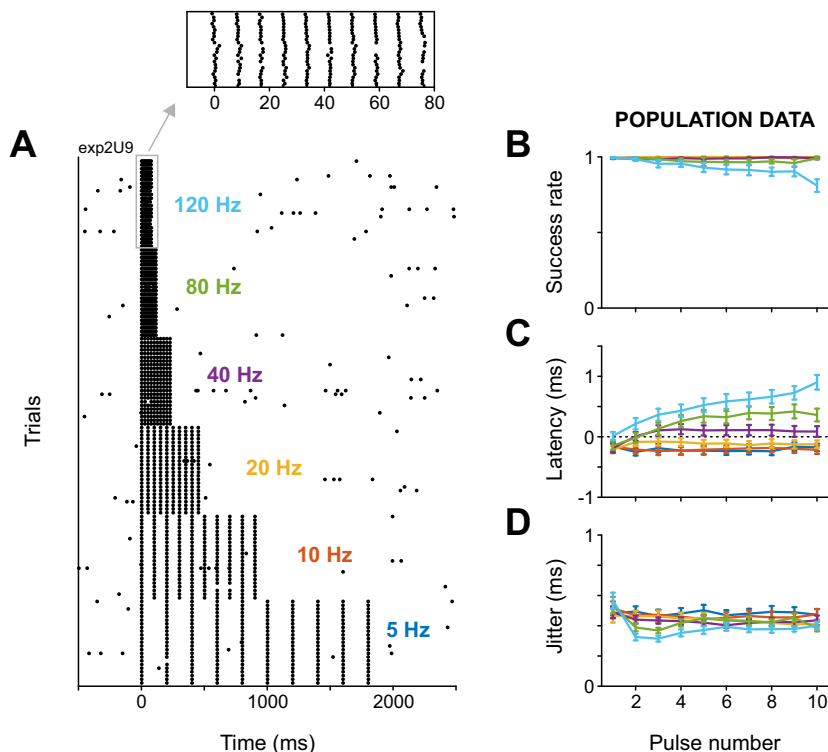


Fig. 3. Kurzpuls trains reliably induce precisely timed spikes at stimulation frequencies up to 120 Hz. *A*: spike raster for an example neuron driven with trains of 10 kurzpulses (amplitude 1.3 T) at stimulation frequencies of 5–120 Hz presented in pseudorandom sequence (repetition rate 0.2 Hz). *Inset* contains a magnified excerpt of the display, illustrating the high temporal precision of evoked spikes in response to kurzpuls trains at 120 Hz. *B*: success rate for each of 10 successive kurzpulses delivered at frequencies of 5–120 Hz (color-coded), and averaged over  $n = 23$  cells. Values are means  $\pm$  SD. *C*: same as *B*, but for spike onset latency. *D*: same as *B*, but for spike time jitter. Average doublet rates were lower than 0.025 for all pulse numbers and frequencies (not shown).

kurzpulses, peak currents were inadvertently reduced by  $<3\%$  for *pulses 2–9* for 80-Hz trains, and peak currents of *pulses 1* and *10* were reduced by 7% for 120-Hz trains. Surprisingly, firing rates exceeding 100 Hz could be consistently realized in all tested presumed excitatory neurons. Average doublet rates were below 0.025 in all cases (data not shown). Spike onset latency remained roughly constant throughout pulse trains at frequencies of 5–120 Hz and subtly increased at frequencies of 40–120 Hz. Spike time jitter stayed low ( $\sim 0.5$  ms) and roughly constant across all stimulation frequencies.

**Induction of natural spike trains.** Cortical neurons generally exhibit highly irregular firing rates, with the CV of interspike intervals approaching 1, especially in early cortical areas (Maimon and Assad 2009; Softky and Koch 1993). To examine whether kurzpuls trains could be used to induce natural-like firing patterns, we tested five additional neurons with Poisson pulse sequences (i.e., trains with exponentially distributed interpulse intervals) featuring target frequencies of 5, 10, 20, and 40 Hz (10 sequential pulses at each frequency). Each neuron was tested repeatedly with the same Poisson 10-pulse

sequence at a particular frequency, but for every experiment on a different neuron, a fresh new Poisson pulse sequence was generated for each target frequency.

The protocol turned out to be highly effective. As visible from Fig. 4, *A–D*, average success rates were close to 1, which held for all 10 pulses in the sequence, regardless of frequency. Spike onset latency relative to the kurzpuls peak was close to 0 ms for 5–20 Hz, but spikes seemed to lag the pulse peak slightly at 40 Hz. However, the average lag amounted to  $<0.5$  ms. More importantly, the temporal precision of spike induction was excellent, with spike time jitter values scattered around 0.5 ms for all target frequencies. This implies that  $\sim 95\%$  of evoked spikes occurred within a time window of  $\pm 1$  ms relative to kurzpuls peaks.

To further challenge the reliability of our spike-induction method, we replayed a 1-min segment of a single-unit recording obtained from a freely moving rat during a texture discrimination task (von Heimendahl et al. 2007). Figure 4*E* shows results from a single neuron recorded at a depth of 919  $\mu\text{m}$  in barrel cortex. Spiking was reliably induced

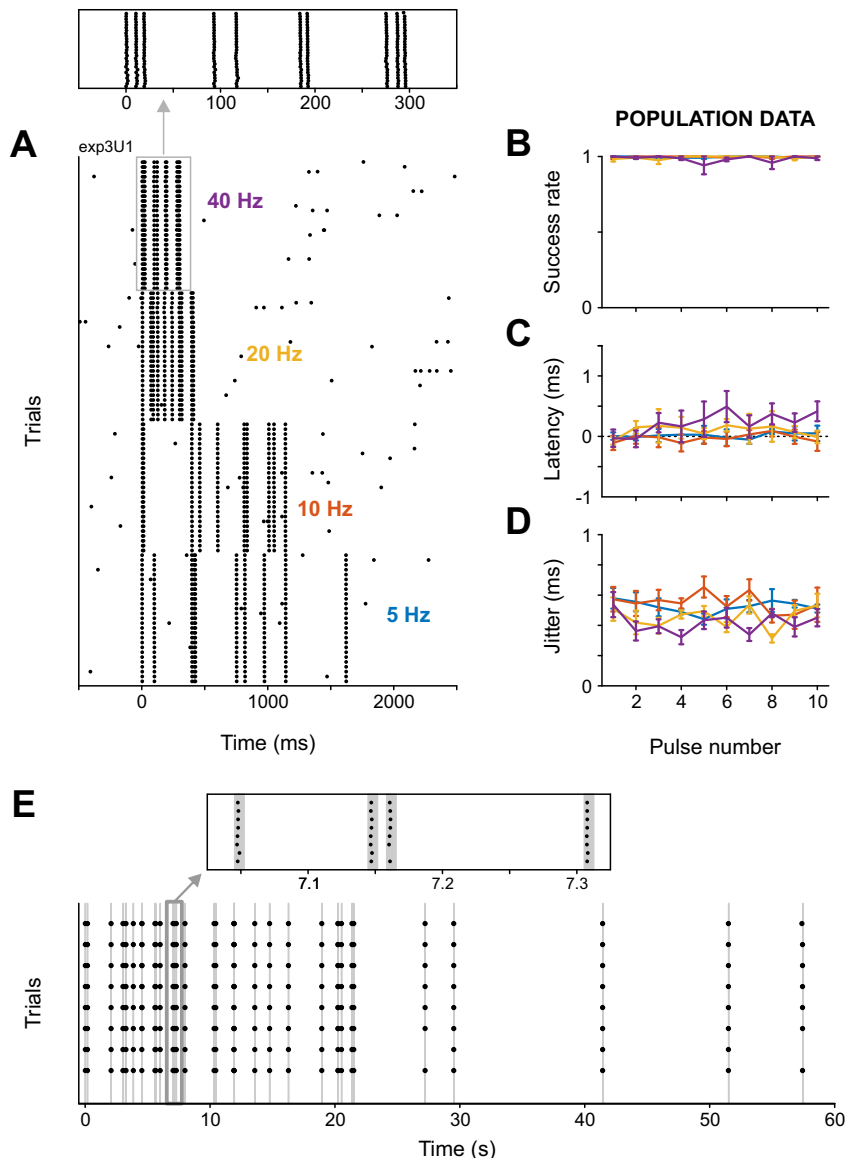


Fig. 4. Kurzpuls nanostimulation can successfully mimic natural spike trains. *A*: spike raster for an example neuron driven with Poisson kurzpuls trains in which pulses (intensity 1.3 T) were separated by random intervals drawn from an exponential distribution. Stimulation frequencies ranged from 5 to 40 Hz and were presented in pseudorandom sequence (repetition rate 0.2 Hz). *Inset* contains a magnified view of spike responses to the first five pulses of a Poisson train at 40 Hz, illustrating the high temporal precision of evoked spikes. *B*: success rates for each of 10 successive kurzpulses, delivered at frequencies of 5–40 Hz (color-coded), and averaged over  $n = 5$  cells. Values are means  $\pm$  SD. Average frequencies of realized 10-pulse sequences varied according to Poisson statistics (means for target frequencies of 5, 10, 20, and 40 Hz were 6.0, 9.6, 23.5, and 30.9 Hz, respectively). *C*: same as *B*, but for spike onset latency. *D*: same as *B*, but for spike time jitter. Average doublet rates were lower than 0.06 for all pulse numbers and frequencies (not shown). *E*: kurzpuls nanostimulation can be used to repeatedly induce a spike train recorded from barrel cortex of a rat performing a whisker-based texture discrimination task. The neuron was driven with kurzpulses at 1.3 T ( $t = 7.5$  nA), and the sequence was replayed 8 times. *Bottom*: spike raster from these 8 trials, each consisting of 36 pulses delivered within 60 s. Shaded vertical lines indicate kurzpuls stimulation. *Top*: highlight of a portion of the sequence with a transiently high firing rate (14 ms between nearest pulses, i.e., 71 Hz).

(>96% of all pulses yielded a spike; no doublets were observed) and with high temporal precision (average spike time jitter: 0.39 ms).

**Whole cell stimulation.** To compare the precision and efficiency of the juxtacellular stimulation technique with whole cell recordings, we collected intracellular data from four cells in which we evoked spikes through rectangular current pulses. Figure 5A shows spike rasters for two cells in which the dependence on current amplitude was tested using 5-ms pulses (as in Fig. 2A). Similar to juxtacellular stimulation, success rate increased with increasing amplitude and reached maximum values around 1.3 T (Fig. 5B). Notably, spikes were frequently induced toward the end of the current pulse or even shortly after stimulus termination; accordingly, we employed analysis windows extending beyond the duration of the pulse (10 ms). Limiting the analysis window to 5 ms yielded reduced

success rates, especially at low current intensities, but had little effect on spike time jitter. Doublet rate was zero throughout for one of the neurons and consistently low for the other. Spike onset latency (relative to current pulse onset) decreased with increasing amplitude for both neurons. The same held for spike time jitter, although this relationship was less obvious for one of the neurons (gray lines). The minimum value of spike time jitter that we achieved with whole cell stimulation (~0.5 ms) is close to that achieved through juxtacellular stimulation (Fig. 2), indicating that the methods are more or less on par in terms of reliability and temporal precision of single-spike induction. In one of the two cells and one other cell, we induced regular spike trains through 5-ms rectangular current pulses at 1.3 T (Fig. 5, C and D). Success rates (using 10-ms analysis windows) were high for all 10 pulses at all frequen-

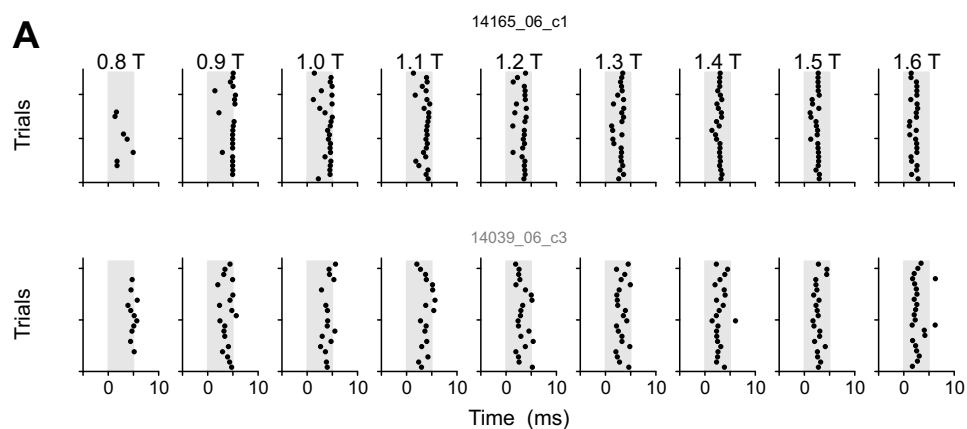
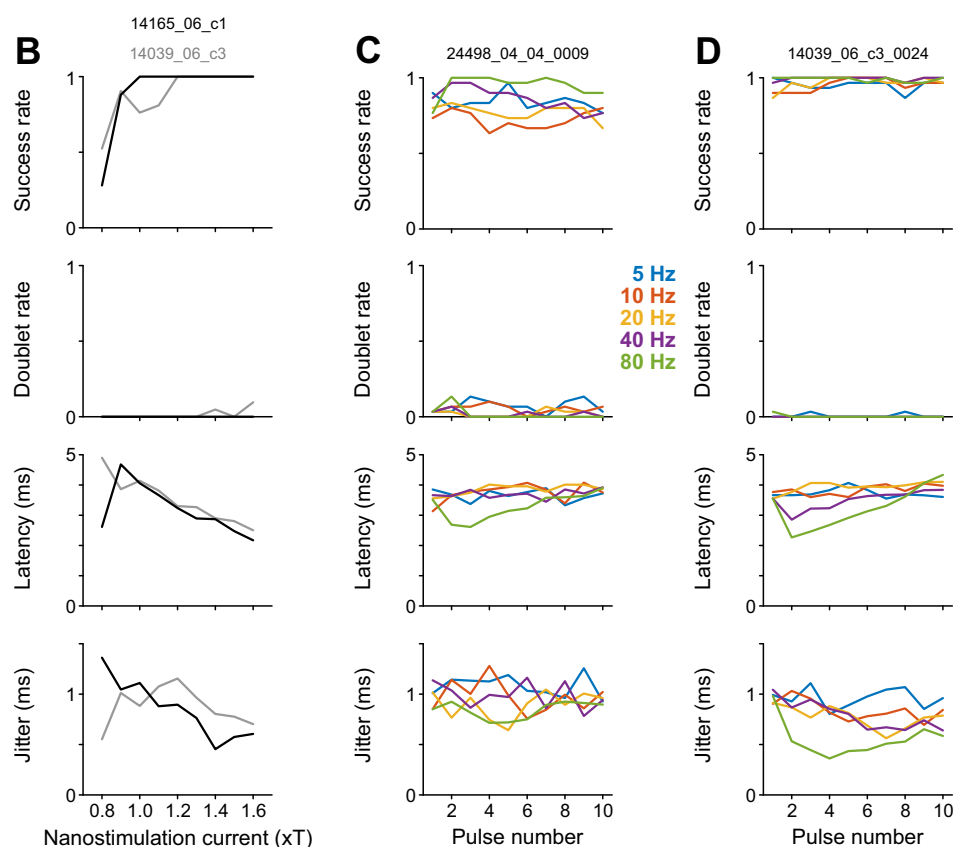


Fig. 5. Reliability and temporal precision of single action potential induction using rectangular 5-ms current pulses in whole cell recordings. **A:** spike rasters for two neurons driven by rectangular 5-ms current pulses (repetition rate 0.4 Hz) at varying current amplitudes, expressed as a factor of threshold current T. Shading highlights the period of current application. **B:** success rate, doublet rate, spike onset latency, and spike time jitter for the two cells shown in A, as a function of current amplitude (solid lines: top; shaded lines: bottom). **C and D:** same as B, but for two cells driven by trains of 10 current pulses (1.3 T, repetition rate 0.2 Hz) at frequencies of 5–80 Hz (color-coded). Data in D and A (bottom row) were obtained from the same cell.





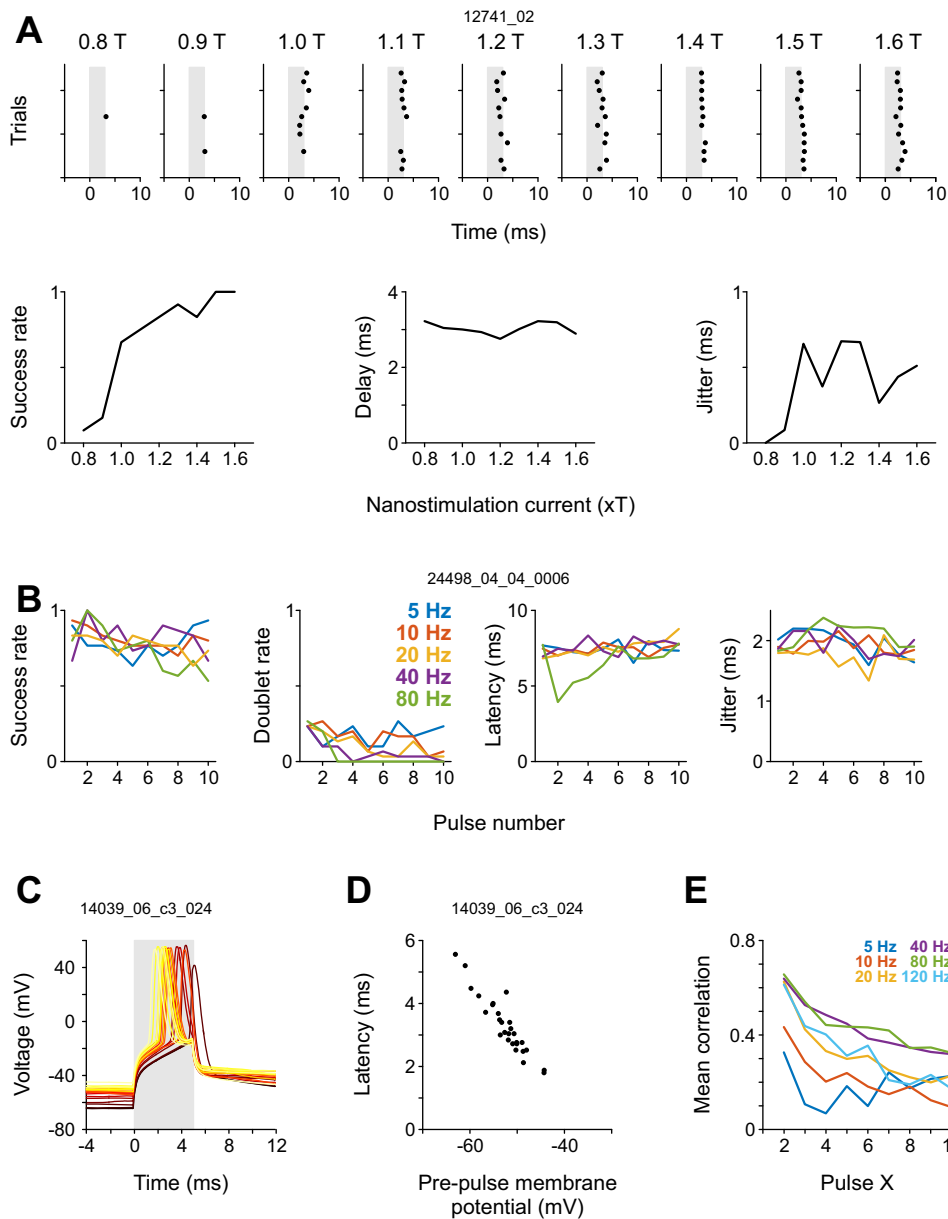


Fig. 6. Reliability and temporal precision of single action potential induction using 3-ms and 10-ms rectangular current pulses in whole cell recordings. **A**: whole cell experiment on a neuron stimulated with 3-ms rectangular pulses delivered at 0.4 Hz. Stimulation current was varied between 0.8 and 1.6 T to assess the current amplitude dependence of spike induction. *Top*: spike raster. Shading indicates stimulus duration. *Bottom*: success rate, spike onset latency, and spike time jitter as a function of current amplitude. Analysis windows were extended to 5 ms to capture spikes immediately following stimulus offset. **B**: whole cell experiment on a neuron stimulated with 10-ms rectangular pulses (1.3 T) arranged in trains of varying frequency (5–80 Hz, constant interpulse intervals, repetition rate 0.2 Hz). Same neuron as in Fig. 5C. Panels show success and doublet rates, spike onset latency, and spike time jitter as a function of pulse number in the train and stimulation frequency (color-coded). Analysis windows were set to 15 ms (results were virtually unaffected by reducing the width to 10 ms). **C–E**: spike onset latency depends on prepulse membrane potential. **C**: membrane potential responses to 20 rectangular current injections (5 ms duration, 1.3 T, repetition rate 0.2 Hz) for a cell recorded in whole cell configuration. Data were taken from the experiment in Fig. 5D; only the first pulse in each pulse train was included for analysis. Color code of traces indicates prepulse membrane potential. **D**: scatterplot illustrating the negative relationship between the membrane potential averaged over a 10-ms period before pulse onset and spike onset latency (same cell as in Fig. 5A). **E**: in kurzpuls nanostimulation experiments with trains of 10 pulses, spike onset times for pulses 2–9 were positively correlated with spike onset time for pulse 1. Plot displays the Pearson correlation between pulse 1 spike onset time and pulse X spike onset time, averaged over  $n = 23$  cells (same data as in Fig. 3). Colors represent stimulation frequencies (5–120 Hz).

cies in one of the neurons, but somewhat variable for the other neuron. For both cells, spike time jitter values varied around a median of 0.9 ms across pulses and frequencies.

We also performed an experiment with 3-ms pulses and one with 10-ms pulses (Fig. 6, *A* and *B*). Both success rate and spike time jitter values were comparable between 3- and 5-ms pulse experiments. In contrast, 10-ms pulses resulted in increased spike time jitter, almost double the size of that obtained with 5-ms pulses. Interestingly, success rates were slightly lower, even though doublet rates increased a bit compared with 5-ms pulses. These experiments suggest that 5-ms pulses are superior to 10-ms pulses, with regard to both precision as well as reliability.

Taken together, these results indicate that the precision achieved with kurzpuls nanostimulation is as good as or better than that with whole cell stimulation, although the latter could potentially be optimized through the use of 3-ms pulses or fluctuating kurzpuls-like current waveforms.

**Determinants of spike time jitter.** Single-spike induction through kurzpuls nanostimulation and whole cell stimulation are both temporally highly precise, with spike time jitter consistently being  $<1$  ms. Given that current pulses were kept identical from trial to trial, spike time jitter might in principle stem from at least four remaining sources: first, distance of the membrane potential to spike threshold; second, fluctuations in input resistance due to synaptic bombardment; third, changes in juxtacellular pipette-cell seal due to movement of the brain; and fourth, cell-intrinsic noise sources (e.g., probabilistic ion channel opening and closing, or dynamic variations in action potential T). Anesthesia induces coordinated activity across cortical networks, which is reflected in the membrane potentials of individual neurons (up/down-states; e.g., Li et al. 2009; Steriade et al. 1993). On the one hand, more depolarized potentials are expected to yield faster spike onsets to current injections due to a reduced distance to spike threshold. On the other hand, more depolarized potentials are accompanied by

reduced Na<sup>+</sup> channel availability and reduced input resistance due to synaptic bombardment (Destexhe et al. 2003), which both predict slower spike onsets. To assess the role of membrane potential, we correlated the prestimulus membrane potential of the cells recorded in whole cell mode to the spike onset latency (Fig. 6, C and D). For the neuron depicted in these two panels, a strong negative correlation is apparent ( $r = -0.94$ ,  $P < 10^{-12}$ ), indicating that more depolarized membrane potentials are associated with earlier spike onsets. This relationship was observed for all tested cells, with Pearson's correlation values ranging from  $-0.76$  to  $-0.95$ . The large proportion of variance explained by prepulse membrane potential ( $r^2 > 80\%$ ) suggests a minor role for other noise sources in determining spike time precision to brief current injections.

In our kurzpuls nanostimulation experiments, spike timing may be similarly affected by prepulse membrane potential. We cannot directly test this hypothesis because we lack access to the prepulse membrane potential in nanostimulation experiments. However, since subthreshold membrane potential varied slowly over time in our whole cell recordings (autocorrelations decayed to zero within 250 ms and then remained slightly negative for hundreds of milliseconds), the influence of the membrane potential on spike onset latency should be visible across consecutive kurzpulses. More specifically, this notion predicts that spike onset latencies should be correlated between consecutive kurzpulses, and the correlation should decrease with the temporal distance between neighboring pulses. This was indeed the case. Figure 6E reveals that spike onset latencies between consecutive kurzpulses (taking the spike onset latency for all first pulses of all trials for a given stimulation frequency and correlating this vector with spike onset latencies for the spikes evoked by the second, third, . . . pulses of all trials for the same stimulation frequency; same data as in Fig. 3) were on average moderately correlated, and the magnitude of the correlation increased with decreasing temporal distance between pulses, both within pulse trains (pulse number) and across pulse trains (pulse train frequency).

Fluctuations in the juxtacellular pipette-cell seal (e.g., due to movement) may constitute another mechanism contributing to the variance in spike onset latency in kurzpuls nanostimulation experiments. The pipette-cell seal affects the flow of amplifier-generated current through intra- and extracellular pathways, such that a larger fraction of injected current enters the cell when the seal resistance ( $R_S$ ) increases (Perkins 2006; Houweling et al. 2010).  $R_S$  was rather stable during our experiments, as indicated by instantaneous total impedance measurements ( $R_T = \Delta V/\Delta I$  during kurzpuls current injections, in the juxtacellular configuration  $R_T \approx R_S + R_p$ , where  $R_p$  indicates pipette resistance), which varied little during experiments (CV: mean 0.036; range: 0.0091–0.079). Consistent with the hypothesis that prepulse membrane potential largely determines spike onset latency, we found low correlations between instantaneous  $R_T$  and spike onset latency in the majority of cells (mean  $r = -0.02$ , range  $-0.47$ – $0.44$ ; based on  $n = 23$  experiments shown in Fig. 3).

We were curious whether juxtacellular potentials could be used similar to intracellular potentials for the prediction of spike onset time. Although subthreshold juxtacellular potential fluctuations display a limited range (SD of prepulse potentials  $< 0.35$  mV in our recordings) and are usually taken to reflect

the local field potential (e.g., Doron et al. 2014), they have been used to quantify subthreshold membrane potential activity (van der Heijden et al. 2013) in agreement with theoretical considerations that, the tighter  $R_S$ , the more the recorded potential reflects the membrane potential (Perkins 2006). In our recordings, however, the average correlation between prepulse juxtacellular potential and spike onset latency was small (mean  $r = -0.13$ , range  $-0.62$ – $0.44$ ) and significant in only 13 out of 23 cells. In 10 of these 13 cells, this correlation was negative, as reported above for the intracellular membrane potential. In this analysis, we quantified prepulse juxtacellular potential as the average potential in a 10-ms window directly preceding kurzpuls onset and subtracted the average potential in a 1-s window directly preceding the prepulse window to correct for drift. Interestingly, the correlation values were themselves inversely correlated with prepulse potential variability ( $r = -0.60$ ,  $P = 0.0026$ ), raising the possibility that, in a subset of neurons (those with a larger range of juxtacellular potentials), juxtacellular potentials partially reflect membrane potential. This could in principle occur either because of a tight seal between the membrane and the tip of the pipette (as discussed above), or because the membrane patch in close vicinity to the pipette tip is rendered leaky by the current pulses. Indeed, increased membrane conductance might even be a prerequisite for achieving precise control over spiking. On the other hand, the negative correlation between prepulse juxtacellular potential and spike onset latency was only observed in a minority of neurons, and these cells were not significantly different from the others with respect to average spike onset latency or spike timing jitter. Moreover, basal firing rates (computed over 1-s intervals preceding kurzpuls trains) did not change significantly across the recording in the majority of cells (19 of 23 neurons shown in Fig. 3), and changes were rather mild in the remaining 4 cells. Moreover, action potential amplitudes and waveforms were stable throughout the stimulation protocols (data not shown). Taken together, our data do not support the hypothesis that significant and persistent membrane leakiness is required for precise control of a cell's action potential output. Instead, we hypothesize that the current pulses induce a highly transient dielectric breakdown of the membrane close to the pipette tip, potentially through the formation of aqueous pores which seal within milliseconds after stimulus offset (see Houweling et al., 2010, for further discussion).

We analyzed a few other possible determinants of spike time jitter, namely the stimulation current threshold  $T$  of a given neuron, the animal's age, mean  $R_T$  across the experiment, and recording depth. None of these variables was significantly related to spike time jitter. Together, these analyses indicate that prestimulus membrane potential is the major determinant of spike time jitter [with the coefficient of determination ( $r^2$ )  $\sim 0.8$ ], and that all other factors potentially affecting spike onset latency together, thus account for  $< 20\%$  of the variance.

*Optogenetic stimulation.* Along with electrical microstimulation, optogenetic stimulation is the most popular method to activate multiple neurons. To compare the efficacy of optogenetic stimulation to kurzpuls nanostimulation, we transfected six animals with AAV2/2-hSyn-ChR2(H134R)-EYFP and performed juxtacellular recordings on several cells during photostimulation. Pilot experiments indicated that cells tolerated our maximum light intensity (80 mW/mm<sup>2</sup> near the brain surface),

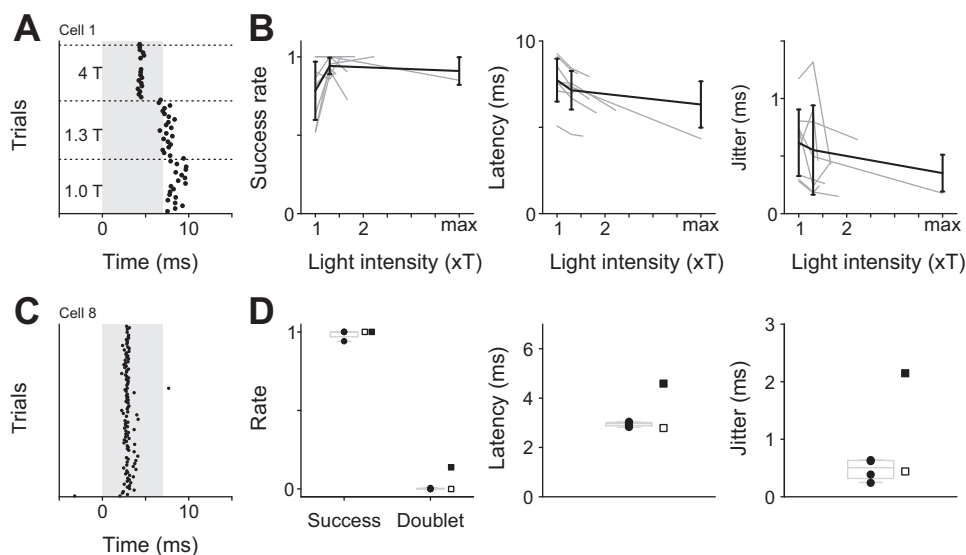


Fig. 7. Light intensity dependence, reliability, and temporal precision of action potentials induced by photostimulation. *A*: spike rasters of an example neuron stimulated with isolated 7-ms light pulses at three different intensities (1.0 T, 1.3 T, and maximum light intensity provided by the LED). *B*: dependence of success rate, spike onset latency, and spike time jitter on light intensity. Doublet rate was zero throughout. Shaded lines: individual neurons; solid lines: mean. Values are means  $\pm$  SD. All neurons in *A* and *B* were recorded while excitatory synaptic transmission was pharmacologically blocked by surface application of APV and CNQX. *C*: spike rasters for an example cell excited by isolated 7-ms light pulses delivered at 0.4 Hz. Shading indicates stimulus duration. *D*: success and doublet rates, spike onset latency, and spike time jitter computed using a 14-ms analysis window originating from light onset. Solid circles indicate data points for each of the four cells stimulated with 7-ms pulses; squares represent the two cells stimulated with 5-ms pulses. Boxplots (light shading) apply to 7-ms light pulse experiments only.

and we, therefore, used maximum light intensity rather than 1.3 T (as in nanostimulation experiments) to achieve maximum success rates and minimum spike time jitter. However, in most cells, success rate and spike time jitter were very similar at 1.3 T and maximal light intensity (Fig. 7, *A* and *B*).

Figure 7, *C* and *D*, shows data from four cells excited with isolated 7-ms light pulses delivered at 0.4 Hz (example neuron in Fig. 7*C*) and two other cells excited with 5-ms light pulses. All four cells excited with 7-ms pulses responded with average spike onset latencies close to 3 ms (range 2.82–3.04 ms), indicative of direct excitation by light pulses (see, e.g., Lima et al. 2009). Success rates ranged from 0.93 to 1, all doublet rates were  $<0.01$ , and spike time jitter ranged from 0.25 to 0.64 ms. In one of the cells excited with isolated 5-ms light pulses, we made very similar observations (Fig. 7*D*, *cell 11*, indicated by open squares), whereas the other cell exposed to 5-ms pulses responded at more variable latencies consistent with indirect excitation (Fig. 7*D*, *cell 10*, indicated by solid squares).

These results indicate that optogenetic stimulation using ChR2(H134R) with isolated light pulses is reliable and temporally precise. Next, we assessed the ability of optogenetic stimulation to induce regular spike trains. The protocol was identical to the above-described nanostimulation experiment in which we induced regular spike trains at 5, 10, 20, and 40 Hz, and we employed identical analyses. We found that success rates were quite high for low-frequency stimulation (5 and 10 Hz), but deteriorated at higher stimulation frequencies (20 and 40 Hz; Fig. 8).

In the above experiments, channelrhodopsin was expressed in multiple cortical neurons, possibly including inhibitory cells (Diester et al. 2011). Thus individual spikes in optogenetic experiments could have resulted from a complex interplay of direct ChR2-mediated excitation and indirect network activity. Focusing on short-latency spikes ( $<4$  ms) occurring during

isolated pulses (Fig. 7) or first pulses in a train mitigates the problem, as these are commonly assumed to directly result from light activation rather than synaptic input (Lima et al. 2009). An alternative approach requires limiting optogenetic stimulation to single cells (Packer et al. 2015; Rickgauer et al. 2014); however, this was beyond the scope of the present study. To better characterize the precision and reliability of directly light-induced spikes in the current experimental setting, we recorded from eight additional cells while applying APV and CNQX on the surface of the brain to block excitatory synaptic transmission (see METHODS). Although blockade of excitatory transmission ensured that cells were excited directly, surprisingly, response latencies were relatively high ( $>5$  ms; Fig. 9) compared with experiments performed without drugs. These increased response latencies might be due to the reduced neuronal excitability following blockade of excitatory synaptic inputs, as indicated by the near complete abolishment of spontaneous firing activity in our recordings.

Nonetheless, results were overall quite similar to previous experiments performed without blockers: success rates were high ( $>0.85$ ) for low-frequency trains (5 and 10 Hz) and deteriorated for higher frequencies. Doublet rates were close to zero throughout, and spike time jitter was  $\sim 0.5$  ms. We conclude that optogenetic stimulation using ChR2(H134R) yields high but suboptimal success rates, at least under our testing conditions, and achieves temporal precision on par with that of kurzpuls nanostimulation (as far as single spikes are concerned). However, ChR2(H134R) is not well suited to induce high-frequency spike trains in vivo using our expression approach.

## DISCUSSION

We here present a method that provides tight control over the spiking output of single cortical neurons in vivo. In nearly

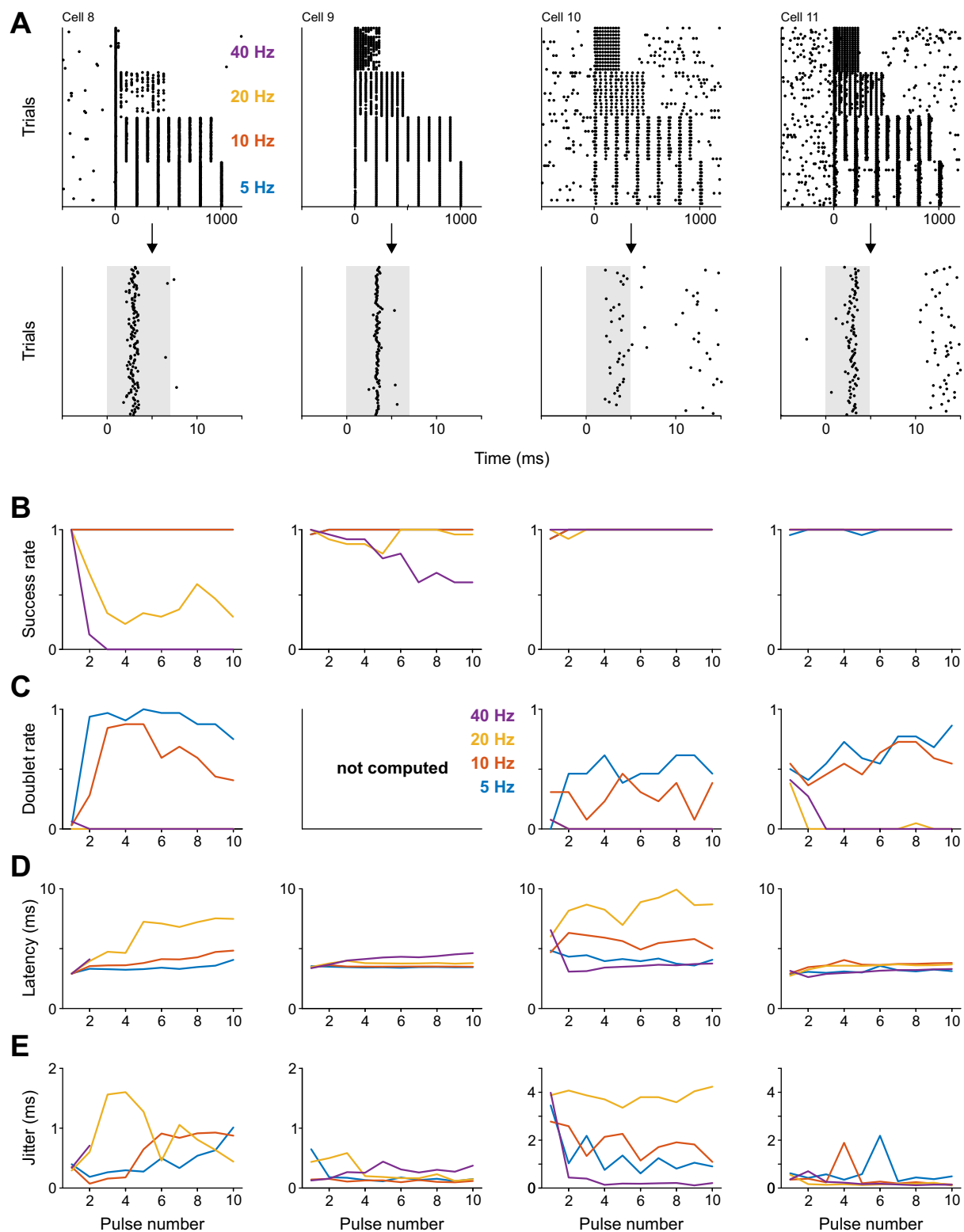


Fig. 8. Photostimulation reliably induces regular spike trains at low but not high frequencies. *A*, *top*: spike rasters of four cells stimulated with sequences of light pulses at 5, 10, 20, and 40 Hz (repetition rate 0.2 Hz). *Bottom*: magnified view of responses to first light pulses. Shading highlights stimulation period. *B–E*: success and doublet rate, spike onset latency, and spike time jitter for each of the four cells (columns) shown in *A*, respectively. Doublets were not scored for *cell 9*. *Cells 8–9* were stimulated with 7-ms light pulses, and *cells 10–11* with 5-ms light pulses. Conventions are as shown in earlier figures.

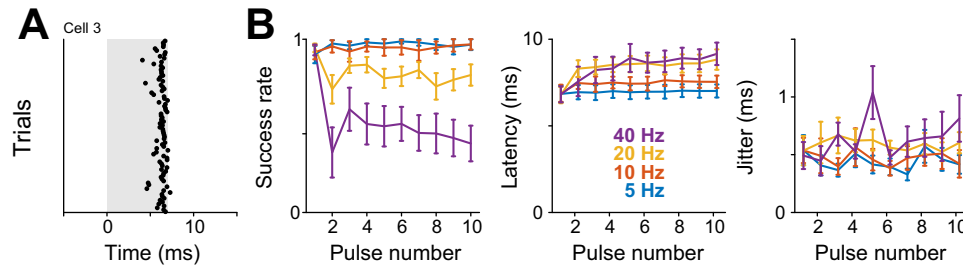


Fig. 9. Blocking excitatory transmission increases onset latency of photostimulation-induced spikes, but has little effect on success rate and spike time jitter. *A*: spike responses of one example cell stimulated with sequences of light pulses at 5, 10, 20, and 40 Hz (repetition rate 0.2 Hz), while excitatory synaptic transmission was pharmacologically blocked by surface application of APV and CNQX. Only responses to first pulses are shown. *B*: success rate, spike onset latency and spike time jitter averaged across eight cells. Doublet rates were near zero throughout. Values are means  $\pm$  SD.

all experiments, we achieved a 1-to-1 coupling of stimulation pulse application and spike generation. Moreover, we could reliably drive cells with high temporal precision ( $\sim 0.5$ -ms spike time jitter) with frequencies up to 120 Hz, regardless of whether these temporal patterns were regular or irregular, or even had been recorded in other animals. Importantly, kurzpuls nanostimulation does not induce stimulation artifacts that may occlude neuronal spikes, as is the case for standard DC nanostimulation, and it can be targeted to single neurons in all layers of cortex as well as other deep brain structures (Houweling et al. 2010).

Temporal patterns of action potentials influence a variety of activity-dependent processes within neurons. For example, expression of the immediate-early gene *c-fos* is regulated by the interval between repeated bursts of action potentials (Fields et al. 2005). Similarly, levels and patterns of neuronal activity influence dendritic growth and branching (McAllister 2000), and a recent study employing photostimulation of cortical layer 5 pyramidal neurons showed that dendritic spine stability depends on the pattern rather than the total amount of induced neural activity (Wyatt et al. 2012). Also, neurons can regulate the position of the axon initial segment (and thereby intrinsic excitability), according to their ongoing levels and patterns of electrical activity (Grubb and Burrone 2010), and homeostatically adjust synaptic input strengths in response to changes in their own firing rate (Goold and Nicoll 2010; Ibata et al. 2008). Temporal patterns of action potentials also influence activity-dependent processes that impact postsynaptic neurons. For example, spike timing-dependent synaptic plasticity is highly dependent on the interval between pre- and postsynaptic spikes, as well as the spiking history of the neurons (Froemke et al. 2006). Up to now, action potential-dependent cellular processes have been primarily investigated in cell cultures and brain slices, and in most cases their operation *in vivo* remains to be elucidated. Kurzpuls nanostimulation may play a pivotal role in this endeavor, as large-scale, global manipulations of neural activity (e.g., sensory deprivation or multicell photostimulation) affect action potential firing as well as synaptic activity in highly complex ways, complicating a mechanistic analysis of the activity-triggered cellular processes.

In a similar vein, kurzpuls nanostimulation is ideally suited to study the effects of single-cell action potential activity on the local microcircuit, movement, and sensation. Even a single extra spike in one layer 5 pyramidal neuron of rat barrel cortex is estimated to produce  $\sim 28$  additional spikes in its postsynaptic targets (London et al. 2010). Single-cell photostimulation of a hippocampal CA1 place cell during behavior perturbs the

spatial firing fields of other place cells (Rickgauer et al. 2014). Moreover, single-cell stimulation induces whisker movement when applied to layer 5/6 pyramidal neurons in rat motor cortex (Brecht et al. 2004) or single motoneurons in the brain stem facial nucleus (Herfst and Brecht 2008). Single-cell stimulation even elicits sensations when applied in rat barrel cortex, as inferred using psychophysical procedures (Houweling and Brecht 2008). In addition, a recent report hints at the possibility that the temporal pattern of action potentials in single neurons of rat barrel cortex affects detectability of single-neuron stimulation (Doron et al. 2014). Unanswered questions related to all of these observations concern the mechanisms of network recruitment by single-neuron action potentials, as well as the role of their temporal patterns. The new kurzpuls nanostimulation method provides a valuable tool for addressing these important questions.

Previous whole cell stimulation studies employed rectangular current pulses (e.g., Kwan and Dan 2012; Li et al. 2009). Similar to DC nanostimulation, this approach does not offer control over the induced spike pattern beyond the approximate average spike number, although it can be used to trigger single spikes (Brecht et al. 2004; London et al. 2010). However, as outlined in the Introduction, *in vivo* whole cell recording is technically challenging and has, therefore, been only rarely employed in awake animals (Crochet and Petersen 2006; Epsztein et al. 2011; Haider et al. 2013). Moreover, whole cell recordings are even more difficult in highly trained animals performing a behavioral task (McGinley et al. 2015; Sachidanandam et al. 2013), and they are low yield, as recordings are limited to a single recording session per animal. In contrast, juxtacellular stimulation is technically less challenging and yields stable recording and stimulation conditions even in well-trained, task-performing animals and over multiple recording sessions (Doron et al. 2014; Houweling and Brecht 2008; Voigt et al. 2008). In addition, our results show that stimulation in whole cell configuration does not offer additional reliability or temporal precision. As for whole cell recordings, nanostimulated neurons can be labeled to allow subsequent anatomical identification (Pinault 1994; Pinault 1996; Tang et al. 2014).

Applied *in vivo*, kurzpuls nanostimulation is limited to one or two single neurons at a time. Optogenetic stimulation approaches are commonly targeted to large neuronal populations, although several single-cell photostimulation approaches are possible. For example, Chr2 can be expressed in single neurons using single-cell electroporation (Kitamura et al. 2008), or sparsely expressed and excited with a focal blue light

beam (Wilson et al. 2012). More recently, approaches for simultaneous two-photon excitation photostimulation and calcium imaging of single neurons have been developed (Packer et al. 2015; Rickgauer et al. 2014). Single-cell photostimulation should be advantageous compared with electrophysiological single-cell stimulation in cases where repeated stimulation of the same cell over multiple sessions is desirable, or stimulation of multiple individually targeted neurons. However, photostimulation at present does not offer additional reliability or temporal precision compared with electrophysiological single-cell stimulation. Current blue light single-pulse photostimulation approaches in vivo provide a temporal precision of induced action potentials of  $<1$  ms (Fig. 7; Kvitsiani et al. 2013; Mateo et al. 2011), but they typically suffer from failures at high stimulation frequencies (Cardin et al. 2009; but see Klapoetke et al. 2014 for recent advances). With two-photon excitation photostimulation, the temporal precision of induced action potentials is low (jitter  $>8$  ms) at this time, repetitive stimulation is limited to relatively low stimulation frequencies (20 Hz) due to saturation of the optogenetic probe (integration time constant of  $\approx 50$  ms for C1V1), and the optical read-out is at relatively low temporal resolution under typical high-speed calcium imaging conditions (15–30 Hz). In contrast, kurzpuls nanostimulation can be used to induce reliable, high-precision (jitter  $\approx 0.5$  ms) spike trains with stimulation frequencies up to 120 Hz. To its disadvantage, single-cell photostimulation may lead to inadvertent stimulation of nontargeted neurons (e.g., due to out-of-focus excitation or illumination of neuronal processes), and imaging illumination may increase spontaneous firing rates in neurons expressing light-sensitive optogenetic probes (Packer et al. 2015; Rickgauer et al. 2014). Moreover, all of the above single-neuron photostimulation approaches require two-photon microscopy and are, therefore, limited to the superficial cortical layers when applied noninvasively.

It is remarkable that single cortical neurons can be induced to fire highly reliable and precise spike trains in vivo, given the continuous bombardment of synaptic activity under in vivo conditions (Destexhe et al. 2003). The precision is considerably higher than in previous experiments on cortical neurons exposed to strong sensory stimulation (e.g., Buračas et al. 1998; Gabernet et al. 2005; Kayser et al. 2010). Spike time precision is comparable to that observed in vitro using low-pass filtered white noise current injections (jitter 1–2 ms) inducing highly reliable spike trains (Mainen and Sejnowski 1995), which is surprising given the increased background synaptic activity and membrane potential variability in vivo (see Doose et al. 2016 for a theoretical analysis of nanostimulation-induced high-frequency spiking). The high precision of action potential induction with kurzpuls nanostimulation (jitter  $\approx 0.5$  ms) does not require extreme current injections. We employed current intensities of 30% above spike T, but precision decreases only slightly for smaller amplitudes near T (jitter  $\approx 0.7$  ms). These data indicate a low intrinsic noise level of spike generation in vivo. The strong dependence of spike onset latency on prepulse membrane potential in our stimulation experiments suggests that membrane potential fluctuation is by far the largest source of noise in cortical neurons affecting spike generation in response to brief transient inputs, such as induced by somatosensory stimulation (Gabernet et al. 2005). Indeed, first spike latencies in visual cortical neurons were

previously shown to correlate with the spontaneous membrane potential immediately preceding visual stimulation (Azouz and Gray 1999). Additionally, the strong negative correlation between spike onset latency and prepulse membrane potential (Fig. 6D), along with the correlation of spike onset latencies across successive kurzpuls (Fig. 6E) suggest a novel indirect method to sample a neuron's membrane potential, by simply taking the spike onset latencies for single pulses to serve as estimate of the magnitude of membrane potential (in relative units, i.e., interpreting short latencies as indication of more depolarized membrane potential).

#### ACKNOWLEDGMENTS

We thank Jochen Spanke for suggesting to low-pass filter stimulus traces, Moritz von Heimendahl for providing spike train data from previously published work, Steven Kushner and Denise Slump for genotyping, and Gerard Borst for helpful comments. All experiments were performed at the Houweling Laboratory in the Department of Neuroscience, Erasmus University Medical Center Rotterdam, The Netherlands.

#### GRANTS

This work was supported by the Netherlands Organization for Scientific Research. M. C. Stüttgen was supported by a 6-mo research scholarship from the German Research Foundation (DFG STU 544/2-1). H. R. A. P. Geis was supported by a Neuro-BSIK grant awarded to Gerard Borst.

#### DISCLOSURES

No conflicts of interest, financial or otherwise, are declared by the author(s).

#### AUTHOR CONTRIBUTIONS

M.C.S., L.J.N., and A.R.H. conceived and designed research; M.C.S., L.J.N., and H.R.A.P.G. performed experiments; M.C.S., L.J.N., and A.R.H. analyzed data; M.C.S., L.J.N., H.R.A.P.G., P.H.T., and A.R.H. interpreted results of experiments; M.C.S. and A.R.H. prepared figures; M.C.S., L.J.N., and A.R.H. drafted manuscript; M.C.S., L.J.N., H.R.A.P.G., P.H.T., and A.R.H. edited and revised manuscript; M.C.S., L.J.N., H.R.A.P.G., P.H.T., and A.R.H. approved final version of manuscript.

#### REFERENCES

- Arabzadeh E, Panzeri S, Diamond ME. Deciphering the spike train of a sensory neuron: counts and temporal patterns in the rat whisker pathway. *J Neurosci* 26: 9216–9226, 2006. doi:10.1523/JNEUROSCI.1491-06.2006.
- Azouz R, Gray CM. Cellular mechanisms contributing to response variability of cortical neurons in vivo. *J Neurosci* 19: 2209–2223, 1999.
- Bair W, Koch C. Temporal precision of spike trains in extrastriate cortex of the behaving macaque monkey. *Neural Comput* 8: 1185–1202, 1996. doi:10.1162/neco.1996.8.6.1185.
- Bi GQ, Poo MM. Synaptic modifications in cultured hippocampal neurons: dependence on spike timing, synaptic strength, and postsynaptic cell type. *J Neurosci* 18: 10464–10472, 1998.
- Bittner KC, Grienberger C, Vaidya SP, Milstein AD, Macklin JJ, Suh J, Tonegawa S, Magee JC. Conjunctive input processing drives feature selectivity in hippocampal CA1 neurons. *Nat Neurosci* 18: 1133–1142, 2015. doi:10.1038/nn.4062.
- Brecht M, Schneider M, Sakmann B, Margrie TW. Whisker movements evoked by stimulation of single pyramidal cells in rat motor cortex. *Nature* 427: 704–710, 2004. doi:10.1038/nature02266.
- Buračas GT, Zador AM, DeWeese MR, Albright TD. Efficient discrimination of temporal patterns by motion-sensitive neurons in primate visual cortex. *Neuron* 20: 959–969, 1998. doi:10.1016/S0896-6273(00)80477-8.
- Cardin JA, Carlén M, Meletis K, Knoblich U, Zhang F, Deisseroth K, Tsai L-H, Moore CI. Driving fast-spiking cells induces gamma rhythm and controls sensory responses. *Nature* 459: 663–667, 2009. doi:10.1038/nature08002.
- Chagas AM, Theis L, Sengupta B, Stüttgen MC, Bethge M, Schwarz C. Functional analysis of ultra high information rates conveyed by rat vibrissal

- primary afferents. *Front Neural Circuits* 7: 190, 2013. doi:10.3389/fncir.2013.00190.
- Crochet S, Petersen CCH.** Correlating whisker behavior with membrane potential in barrel cortex of awake mice. *Nat Neurosci* 9: 608–610, 2006. doi:10.1038/nm1690.
- Destexhe A, Rudolph M, Paré D.** The high-conductance state of neocortical neurons in vivo. *Nat Rev Neurosci* 4: 739–751, 2003. doi:10.1038/nrn1198.
- DeWeese MR, Wehr M, Zador AM.** Binary spiking in auditory cortex. *J Neurosci* 23: 7940–7949, 2003.
- Diamantaki M, Frey M, Preston-Ferrer P, Burgalossi A.** Priming spatial activity by single-cell stimulation in the dentate gyrus of freely moving rats. *Curr Biol* 26: 536–541, 2016. doi:10.1016/j.cub.2015.12.053.
- Diester I, Kaufman MT, Mogri M, Pashaie R, Goo W, Yizhar O, Ramakrishnan C, Deisseroth K, Shenoy KV.** An optogenetic toolbox designed for primates. *Nat Neurosci* 14: 387–397, 2011. doi:10.1038/nn.2749.
- Domnisoru C, Kinkhabwala AA, Tank DW.** Membrane potential dynamics of grid cells. *Nature* 495: 199–204, 2013. doi:10.1038/nature11973.
- Doose J, Doron G, Brecht M, Lindner B.** Noisy juxtacellular stimulation in vivo leads to reliable spiking and reveals high-frequency coding in single neurons. *J Neurosci* 36: 11120–11132, 2016. doi:10.1523/JNEUROSCI.0787-16.2016.
- Doron G, von Heimendahl M, Schlattmann P, Houweling AR, Brecht M.** Spiking irregularity and frequency modulate the behavioral report of single-neuron stimulation. *Neuron* 81: 653–663, 2014. doi:10.1016/j.neuron.2013.11.032.
- Eguchi M, Yamaguchi S.** In vivo and in vitro visualization of gene expression dynamics over extensive areas of the brain. *Neuroimage* 44: 1274–1283, 2009. doi:10.1016/j.neuroimage.2008.10.046.
- Epszstein J, Brecht M, Lee AK.** Intracellular determinants of hippocampal CA1 place and silent cell activity in a novel environment. *Neuron* 70: 109–120, 2011. doi:10.1016/j.neuron.2011.03.006.
- Fields RD, Lee PR, Cohen JE.** Temporal integration of intracellular Ca<sup>2+</sup> signaling networks in regulating gene expression by action potentials. *Cell Calcium* 37: 433–442, 2005. doi:10.1016/j.ceca.2005.01.011.
- Frommke RC, Tsay IA, Raad M, Long JD, Dan Y.** Contribution of individual spikes in burst-induced long-term synaptic modification. *J Neurophysiol* 95: 1620–1629, 2006. doi:10.1152/jn.00910.2005.
- Gabernet L, Jadhav SP, Feldman DE, Carandini M, Scanziani M.** Somatosensory integration controlled by dynamic thalamocortical feed-forward inhibition. *Neuron* 48: 315–327, 2005. doi:10.1016/j.neuron.2005.09.022.
- Goold CP, Nicoll RA.** Single-cell optogenetic excitation drives homeostatic synaptic depression. *Neuron* 68: 512–528, 2010. doi:10.1016/j.neuron.2010.09.020.
- Grubb MS, Burrone J.** Activity-dependent relocation of the axon initial segment fine-tunes neuronal excitability. *Nature* 465: 1070–1074, 2010. doi:10.1038/nature09160.
- Haider B, Häusser M, Carandini M.** Inhibition dominates sensory responses in the awake cortex. *Nature* 493: 97–100, 2013. doi:10.1038/nature11665.
- Herfst LJ, Brecht M.** Whisker movements evoked by stimulation of single motor neurons in the facial nucleus of the rat. *J Neurophysiol* 99: 2821–2832, 2008. doi:10.1152/jn.01014.2007.
- Houweling AR, Brecht M.** Behavioural report of single neuron stimulation in somatosensory cortex. *Nature* 451: 65–68, 2008. doi:10.1038/nature06447.
- Houweling AR, Doron G, Voigt BC, Herfst LJ, Brecht M.** Nanostimulation: manipulation of single neuron activity by juxtacellular current injection. *J Neurophysiol* 103: 1696–1704, 2010. doi:10.1152/jn.00421.2009.
- Ibata K, Sun Q, Turrigiano GG.** Rapid synaptic scaling induced by changes in postsynaptic firing. *Neuron* 57: 819–826, 2008. doi:10.1016/j.neuron.2008.02.031.
- Johnson DH.** The relationship between spike rate and synchrony in responses of auditory-nerve fibers to single tones. *J Acoust Soc Am* 68: 1115–1122, 1980. doi:10.1121/1.384982.
- Kayser C, Logothetis NK, Panzeri S.** Millisecond encoding precision of auditory cortex neurons. *Proc Natl Acad Sci USA* 107: 16976–16981, 2010. doi:10.1073/pnas.1012656107.
- Kitamura K, Judkewitz B, Kano M, Denk W, Häusser M.** Targeted patch-clamp recordings and single-cell electroporation of unlabeled neurons in vivo. *Nat Methods* 5: 61–67, 2008. doi:10.1038/nmeth1150.
- Klapoetke NC, Murata Y, Kim SS, Pulver SR, Birdsey-Benson A, Cho YK, Morimoto TK, Chuong AS, Carpenter EJ, Tian Z, Wang J, Xie Y, Yan Z, Zhang Y, Chow BY, Surek B, Melkonian M, Jayaraman V, Constantine-Paton M, Wong GK-S, Boyden ES.** Independent optical excitation of distinct neural populations. *Nat Methods* 11: 338–346, 2014. doi:10.1038/nmeth.2836.
- Kvitsiani D, Ranade S, Hangya B, Taniguchi H, Huang JZ, Kepecs A.** Distinct behavioural and network correlates of two interneuron types in prefrontal cortex. *Nature* 498: 363–366, 2013. doi:10.1038/nature12176.
- Kwan AC, Dan Y.** Dissection of cortical microcircuits by single-neuron stimulation in vivo. *Curr Biol* 22: 1459–1467, 2012. doi:10.1016/j.cub.2012.06.007.
- Lee D, Lin B-J, Lee AK.** Hippocampal place fields emerge upon single-cell manipulation of excitability during behavior. *Science* 337: 849–853, 2012. doi:10.1126/science.1221489.
- Li C-YT, Poo M-M, Dan Y.** Burst spiking of a single cortical neuron modifies global brain state. *Science* 324: 643–646, 2009. doi:10.1126/science.1169957.
- Lima SQ, Hromádka T, Znamenskiy P, Zador AM.** PINP: a new method of tagging neuronal populations for identification during in vivo electrophysiological recording. *PLoS One* 4: e6099, 2009. doi:10.1371/journal.pone.0006099.
- Lin JY.** A user's guide to channelrhodopsin variants: features, limitations and future developments. *Exp Physiol* 96: 19–25, 2011. doi:10.1113/expphysiol.2009.051961.
- London M, Roth A, Beeren L, Häusser M, Latham PE.** Sensitivity to perturbations in vivo implies high noise and suggests rate coding in cortex. *Nature* 466: 123–127, 2010. doi:10.1038/nature09086.
- Maimon G, Assad JA.** Beyond Poisson: increased spike-time regularity across primate parietal cortex. *Neuron* 62: 426–440, 2009. doi:10.1016/j.neuron.2009.03.021.
- Mainen ZF, Sejnowski TJ.** Reliability of spike timing in neocortical neurons. *Science* 268: 1503–1506, 1995. doi:10.1126/science.7770778.
- Mateo C, Avermann M, Gentet LJ, Zhang F, Deisseroth K, Petersen CCH.** In vivo optogenetic stimulation of neocortical excitatory neurons drives brain-state-dependent inhibition. *Curr Biol* 21: 1593–1602, 2011. doi:10.1016/j.cub.2011.08.028.
- McAllister AK.** Cellular and molecular mechanisms of dendrite growth. *Cereb Cortex* 10: 963–973, 2000. doi:10.1093/cercor/10.10.963.
- McGinley MJ, David SV, McCormick DA.** Cortical membrane potential signature of optimal states for sensory signal detection. *Neuron* 87: 179–192, 2015. doi:10.1016/j.neuron.2015.05.038.
- Packer AM, Russell LE, Dagleish HWP, Häusser M.** Simultaneous all-optical manipulation and recording of neural circuit activity with cellular resolution in vivo. *Nat Methods* 12: 140–146, 2015. doi:10.1038/nmeth.3217.
- Perkins KL.** Cell-attached voltage-clamp and current-clamp recording and stimulation techniques in brain slices. *J Neurosci Methods* 154: 1–18, 2006. doi:10.1016/j.jneumeth.2006.02.010.
- Pinault D.** Golgi-like labeling of a single neuron recorded extracellularly. *Neurosci Lett* 170: 255–260, 1994. doi:10.1016/0304-3940(94)90332-8.
- Pinault D.** A novel single-cell staining procedure performed in vivo under electrophysiological control: morpho-functional features of juxtacellularly labeled thalamic cells and other central neurons with biocytin or Neurobiotin. *J Neurosci Methods* 65: 113–136, 1996. doi:10.1016/0165-0270(95)00144-1.
- Reinagel P, Reid RC.** Temporal coding of visual information in the thalamus. *J Neurosci* 20: 5392–5400, 2000.
- Rickgauer JP, Deisseroth K, Tank DW.** Simultaneous cellular-resolution optical perturbation and imaging of place cell firing fields. *Nat Neurosci* 17: 1816–1824, 2014. doi:10.1038/nn.3866.
- Sachidhanandam S, Sreenivasan V, Kyriakatos A, Kremer Y, Petersen CCH.** Membrane potential correlates of sensory perception in mouse barrel cortex. *Nat Neurosci* 16: 1671–1677, 2013. doi:10.1038/nn.3532.
- Shadlen MN, Newsome WT.** The variable discharge of cortical neurons: implications for connectivity, computation, and information coding. *J Neurosci* 18: 3870–3896, 1998.
- Softky WR, Koch C.** The highly irregular firing of cortical cells is inconsistent with temporal integration of random EPSPs. *J Neurosci* 13: 334–350, 1993.
- Stellwagen D, Shatz CJ.** An instructive role for retinal waves in the development of retinogeniculate connectivity. *Neuron* 33: 357–367, 2002. doi:10.1016/S0896-6273(02)00577-9.
- Steriade M, Nuñez A, Amzica F.** A novel slow (< 1 Hz) oscillation of neocortical neurons in vivo: depolarizing and hyperpolarizing components. *J Neurosci* 13: 3252–3265, 1993.
- Stüttgen MC, Schwarz C.** Psychophysical and neurometric detection performance under stimulus uncertainty. *Nat Neurosci* 11: 1091–1099, 2008. doi:10.1038/nn.2162.

- Svoboda K, Yasuda R.** Principles of two-photon excitation microscopy and its applications to neuroscience. *Neuron* 50: 823–839, 2006. doi:[10.1016/j.neuron.2006.05.019](https://doi.org/10.1016/j.neuron.2006.05.019).
- Tang Q, Brecht M, Buzsáki A.** Juxtacellular recording and morphological identification of single neurons in freely moving rats. *Nat Protoc* 9: 2369–2381, 2014. doi:[10.1038/nprot.2014.161](https://doi.org/10.1038/nprot.2014.161).
- Tsodyks MV, Markram H.** The neural code between neocortical pyramidal neurons depends on neurotransmitter release probability. *Proc Natl Acad Sci USA* 94: 719–723, 1997. doi:[10.1073/pnas.94.2.719](https://doi.org/10.1073/pnas.94.2.719).
- van der Heijden M, Lorteije JAM, Plauška A, Roberts MT, Golding NL, Borst JGG.** Directional hearing by linear summation of binaural inputs at the medial superior olive. *Neuron* 78: 936–948, 2013. [Erratum. *Neuron* 79: 207, 2013.] [10.1016/j.neuron.2013.04.028](https://doi.org/10.1016/j.neuron.2013.04.028).
- Voigt BC, Brecht M, Houweling AR.** Behavioral detectability of single-cell stimulation in the ventral posterior medial nucleus of the thalamus. *J Neurosci* 28: 12362–12367, 2008. doi:[10.1523/JNEUROSCI.3046-08.2008](https://doi.org/10.1523/JNEUROSCI.3046-08.2008).
- von Heimendahl M, Itskov PM, Arabzadeh E, Diamond ME.** Neuronal activity in rat barrel cortex underlying texture discrimination. *PLoS Biol* 5: e305, 2007. doi:[10.1371/journal.pbio.0050305](https://doi.org/10.1371/journal.pbio.0050305).
- Wilson NR, Runyan CA, Wang FL, Sur M.** Division and subtraction by distinct cortical inhibitory networks in vivo. *Nature* 488: 343–348, 2012. doi:[10.1038/nature11347](https://doi.org/10.1038/nature11347).
- Wyatt RM, Tring E, Trachtenberg JT.** Pattern and not magnitude of neural activity determines dendritic spine stability in awake mice. *Nat Neurosci* 15: 949–951, 2012. doi:[10.1038/nn.3134](https://doi.org/10.1038/nn.3134).

